M-Blocks: Three Dimensional Modular Self-Reconfigurable Robots

by

John William Romanishin

Submitted to the Department of Mechanical Engineering
in partial fulfillment of the requirements for the degree of

Master of Science

at the

MASSACHUSETTS INSTITUTE OF TECHNOLOGY

June 2018

Signature redacted

Author . . . .
Department of Mechanical Engineering
May 17 2018

Signature redacted

Certified by . . . .
Daniela Rus
Andrew (1956) and Erna Viterbi Professor of Electrical Engineering and
Computer Science and Director of CSAIL
Thesis Supervisor

Signature redacted

Certified by . . . .
Amos Winter
Assistant professor
Thesis Supervisor

Signature redacted

Accepted by. . . . .
Rohan Abeyaratne
Quentin Berg Professor of Mechanics, Graduate Officer

M-Blocks: Three Dimensional Modular Self-Reconfigurable Robots

by

John William Romanishin

Submitted to the Department of Mechanical Engineering
on May 17 2018, in partial fulfillment of the
requirements for the degree of
Master of Science

Abstract

This thesis details the development of the 3D M-Blocks modular robot system. Modular self-reconfigurable robots (MSRR) are robotic systems which contain many modules that can form and break connections with other modules, and move on a lattice of other modules in order to form different configurations. The 3D M-Blocks is a new system which attempts to investigate the feasibility of using inertial actuation from reaction wheels in order to pivot modules on a 3D lattice. Many existing systems described in related literature are able to exhibit reconfiguration, but usually these systems are only able to do so under limited circumstances, e.g. they only work in 2 dimensions or in the absence of gravity. The 3D M-blocks is one of the only systems which is able to move modules according to a general lattice movement model in full three dimensional space under the effects of gravity.

The 3D M-Blocks rotate relative to one another through the use of temporary magnetic hinges, and form bonds with each other through the use of permanent magnets. Rules describing the movement framework under which the modules move, called the Pivoting Cube Model (PCM), are discussed in depth. Each 50 *mm* 3D M-Block module contains all of the components necessary to operate autonomously and communicate over WiFi. Each module contains a cubic frame which supports the rotation and magnetic bonding with neighbors, and which holds the core robot assembly, including an inertial actuator and electronics. The inertial actuator is a reaction wheel with a fast acting band brake which is used to generate pulses of torque sufficient to induce lattice pivoting motions.

Experiments characterizing the performance of the inertial actuator and the magnetic hinges are described. Additionally, experiments validating individual lattice movements demonstrate the feasibility of this approach to general 3D reconfiguration. Experiments describing modules modules individually and as groups are also presented.

Thesis Supervisor: Daniela Rus
Title: Andrew (1956) and Erna Viterbi Professor of Electrical Engineering and Computer Science and Director of CSAIL

Thesis Supervisor: Amos G. Winter, V
Title: Assistant Professor of Mechanical Engineering

3

Acknowledgments

Contents

List of Figures

List of Tables

Chapter 1

Introduction

The concepts in the field of Modular Self-Reconfigurable Robotics (MSRR) have captured the imagination of many people. The vision of many hundreds or thousands of robots working in harmony to construct larger robots and structures has been the goal of many researchers for decades, and has appeared in many works of popular science fiction. While dreams of chairs transforming into couches on demand, or bridges reconstructing themselves after natural disasters may seem far-fetched, the foundations for eventually realizing these goals are being created through academic research in this field.

The concepts of modularity and reconfiguration are important in both biological and engineered systems. Life itself is based on multiple layers of modular building blocks, e.g. DNA, amino acids, and genes. These smaller components are rearranged (through somewhat magical-seeming ways) to create a significant diversity of forms and capabilities. Software engineering is likewise built on a foundation of modularity; segments of code can be abstracted away and reused as smaller building blocks in order to create useful software. In theory, the benefits of systems with high levels of modularity include an ease of developing new designs, the ability to repair damaged components, and an ability for modular systems to upgrade and adapt to new circumstances. However there are also significant costs to modularity. As a general rule, the more deeply modularity is ingrained into a system, the lower its performance on certain metrics, e.g. cost, power to weight, speed, etc... will be compared to an optimized design. The primary cause of these performance trade-offs are the redundancy that is introduced by the necessity of having interfaces between the

modular components. These costs are higher in physical systems than in software systems, which might help explain the relative lack of systems based on a substantially modular architecture in the mechanical domain and especially in robotics. The necessary ingredient to overcome these costs and make practical modular robotic systems could be the ability to reconfigure the elements on demand that the MSRR field intends to develop.

Modular Self-Reconfigurable Robotics as a research field has been active since the 1980's, and has seen significant growth since then. There have been many different physical systems presented, at varying levels of development, e.g. M-Tran [42], Robotic Molecule [33], and more described in Section 2.1. There also has been substantial work in the theoretical realm including the creation of different sets of rules for modules to move relative to each other, i.e. *movement frameworks*, and accompanying algorithms for reconfiguration modules according to the rules prescribed by the movement frameworks. The most common movement framework is called the Sliding Cube Model [18], which models the modules as cubes which can can perform sliding motions in any direction relative to other units. However, very few of the mechanical systems which have been presented are actually able to implement these movement frameworks. Usually the actual systems only following a simplified or scaled down version of the framework, leaving implementation of the full model to future work. This mismatch between hardware and software calls out for investigating new methods of movement that are more capable, simpler, and more reliable than those previously implemented in order to further advance the state of the art.

This masters thesis covers the development of the 3D M-Blocks system, which is an attempt to further the MSRR field by investigating the feasibility a novel reconfiguration framework and actuation method for MSRR systems. The thesis details three primary contributions; (1) Development of a new movement model called the 3D Pivoting Cube Model (PCM) and associated hardware which allows these movements. The PCM defines a set of constrains where modules rotate about hinges on each edge of a cubic module, and is described in Chapter 3. (2) Design of a reaction wheel based actuator which is able to move the robots on a 3D lattice. And (3), Creation and testing of a system of 16 3D M-Blocks robots. In the course of working on the 3D M-Blocks system many of the significant challenges involved in creating MSRR systems have come to light. Finally

these challenges and many important engineering lessons learned through trial and error are discussed in Chapter 6.

1.1　3D M-Blocks Project Vision and Overview

<div align="center">(a)　　　　　　　　　　(b)</div>
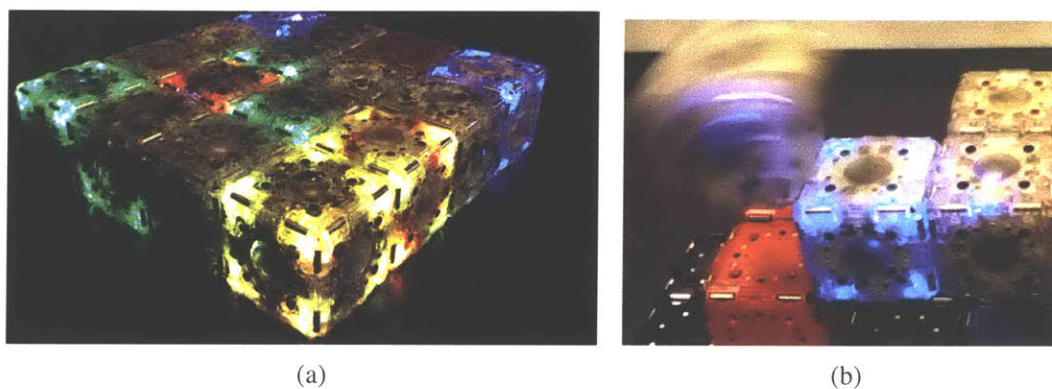
Figure 1-1: (a) Complete set of 16 3D M-Blocks modular robots connected in a 4x4x1 configuration. The colored LEDs in each corner are used to display the internal state of the robots. (b) A 3D M-Block (*blurred, image left*) moves into new lattice position by pivoting about a permanent magnetic hinge on the edge of another module (*blue corners*).

The goal of this research is to demonstrate that modular self-reconfigurable robots propelled by inertial actuation on a cubic lattice moving according to the 3D Pivoting Cube Model is a promising foundation for future large scale modular robotic systems. This project is a continuation of the quest to create autonomous shape-changing robots which are able to change their configuration in order to accomplish different tasks. The long term goal is to create a system with thousands of modules which are able to work together to assemble into useful structures. In order to achieve this vision the focus is on creating a system that is simple, inexpensive, and robust. Simplicity is important in the design of the connector and movement specifications in order to allow the system to take advantage of existing algorithmic developments while being able to be manufactured at a reasonable expense.

Although there are many existing modular robot systems, few of them are able to implement general algorithms based on the standard movement models presented in the literature. One of the reasons why existing systems struggle to implement these algorithms

is due to the problems introduced by symmetry and the sheer number of possible orientations and movements required for general 3D reconfiguration. Assuming a cubic lattice based module with a connector on each of its six faces which attempts to perform both horizontal traversal moves in addition to corner traversal moves (8 moves in total) in North, South, East and West directions, there are up to 48 possible physically distinct movement sequences. While most designs will be able to take advantage of some degree of symmetry in using actuators to generate these movements, most of the mechanical designs presented to date require the use of many (6+) actuators, and often still don't allow full 3D lattice reconfiguration. This proliferation of actuators, in addition to the need to carry computation, batteries, etc, quickly leads to designs that are too heavy, complicated, and fragile to be practical.

The 3D M-Blocks project started out as an attempt to imagine a system using an absolute minimum number of actuators while still allowing motion in three dimensions. The critical research contribution from this project is the realization that instead of applying forces or torques at the connection interfaces between modules, an inertial torque can be applied to the center of mass thereby taking advantage of symmetry to reduce the required mechanical complexity. There are also many initially unforeseen advantages to using inertial actuation. Since the torques are generated internally, the structure of the robot can be closed and hermetically sealed from the environment. The design does not include any actuated external moving components or surfaces requiring support from bearings, both of which are prone to failure. Using inertial forces also makes it simpler for a single module to move on a lattice without assistance or coordination from other modules, which allows for simpler electronics and communication systems to be implemented. Specifically this thesis discusses the following contributions to the research field:

1. Development of the 3D Pivoting Cube Model theory and associated hardware.

2. Design of a pulsed reaction wheel inertial actuator to actuate module movements.

3. Fabrication of a system of 16 modules capable of 3D lattice reconfiguration.

Each 3D M-Block is a 50 mm cubic module with six identical connectors on each of its faces, and no actively driven external parts. While the original M-Block modules presented

in 2013 [49] proved that the inertial actuation and magnetic hinge concept was viable, these modules were capable of movement in just one direction along only one plane. In contrast, the 3D M-Blocks are capable of applying torques in both forward and backward directions along any of the module's three mutually orthogonal planes by introducing a mechanism to reorient the inertial actuator relative to the frame. This allows the modules to move in three distinct fashions: (1) relative to other fixed modules in order to self-reconfigure a larger lattice structure, (2) independently in various environments; and (3) simultaneously as part of an assembly of modules (e.g. all units in spherical meta-modules can roll simultaneously).

The 3D M-Blocks system has many favorable characteristics relative to the state of the art in the MSRR field. One of the most significant advantages is the simplicity of lattice movements. The 3D M-Blocks are one of the only systems in which a single module can move completely independently on a lattice structure, i.e. without direct coordination with surrounding modules. This low communication overhead not only simplifies the algorithmic complexity of movements, but also allows the system to easily reconfigure on a lattice of passive (or disabled) modules. Reconfiguring between even relatively simple structures can require hundreds or thousands of individual movements, therefore the time that each movement takes is important for creating a practically useful system. 3D M-Blocks takes between 1 and 5 seconds to perform lattice movements (depending on difficulty of the movement), which is faster than most of the other MSRR system proposed in related work. The 3D M-Blocks are also one of the only systems which can reconfigure according to a simple movement framework in an unconstrained 3D lattice (although with the current hardware certain particular moves are impractical). The combination of these characteristics will hopefully help create future systems which can achieve the dream of practical reconfigurable robots and structures. Specific examples of systems which this research would be most applicable to include building temporary infrastructure, e.g. a temporary staircase in a disaster environment, and reconfigurable structures in space, e.g. reconfigurable space telescopes.

17

1.2 Thesis organization and Publications

This thesis is based on the following academic papers which include contributions from several people. The following enumerates the research papers that are part of this work (With **bold** indicating primary authorship).

1. **(2013) M-Blocks, Momentum-driven Magnetic Modular Robots** [49]

2. (2015) Reconfiguration Planning for Pivoting Cube Modular Robots [61]

3. **(2015) 3D M-Blocks, Self-reconfiguring Robots Capable of Locomotion via Pivoting in Three Dimensions** [48]

4. (2017) Distributed Aggregation for Modular Robots in the Pivoting Cube Model [14]

This thesis is organized as follows. Chapter 2 gives an overview of related work in two separate fields, beginning with an overview of MSRR systems, discussing each of the major movement framework in detail and ending with a section regarding inertial actuation in robotic systems. Chapter 3 begins by presenting the 3D Pivoting Cube Model (PCM) movement framework, and provides a cursory look at the dynamics involved with applying this framework to physical hardware. This chapter is based on work from [49] and from [61]. Chapter 4 describes the mechanical and electrical design of the 3D M-Blocks system, and is heavily based on the 2015 paper presented in 2015 [48]. Next, Section 5 presents data characterizing the hardware and the results of experiments with the system, drawing upon more recent work, as well as from [48] and from [14]. Finally, Section 6 concludes with a short discussion about the 3D M-Blocks system, reflections on lessons learned and ideas for future work. An Alternate view of the structure of the thesis can be referenced according to Figure 1-2 which organizes the topics according to the three primary research contribution areas presented in this thesis.

	Pivoting Framework	Inertial Actuator	M-Blocks System
Related Work	Other Frameworks **Section 2.1.1-3**	Inertial Actuation **Section 2.2**	MSRR Systems **Section 2.1**
Theoretical Foundation	Pivoting Cube Model **Section 3.1**	Actuator Model **Section 3.2**	
Design and Fabrication	Frame Design **Section 4.4**	Actuator Design **Section 4.3**	Design Overview **Section 4.1**
System Experiments		Actuator Characterization **Section 5.1.1**	System Experiments **Section 5.2**
Discussion		Actuator Improvements **Section 6.3**	Discussion **Chapter 6**

Figure 1-2: This figure presents an alternate view of the structure of this thesis, grouped by main area (or research 'pillar') of contribution. The first research pillar describes the set of rules which guide the reconfiguration of the 3D M-Blocks called the *3D Pivoting Cube Model*. The second pillar regards inertial actuation, which is the method used to actuate 3D M-Block modules. This covers related work, and the design and characterization of a compact reaction wheel-based inertial actuator. The third pillar regards the fabrication and design of the system of multiple 3D M-Block modules.

Chapter 2

Related Work

This thesis relates to work in two primary fields of robotics, including that of Modular Self-Reconfigurable Robotics (MSRR) in addition to inertially actuated robotics. Section 2.1 will provide an overview of the the field of MSRR, and then provide a more detailed look at some the various different movement frameworks and related hardware. Section 2.2 will provide a short introduction into the concept of inertial actuation, followed by a discussion of different robotic systems utilizing it for providing locomotion.

2.1 Modular Self-Reconfigurable Robotics (MSRR)

The goal of the Modular Self-Reconfigurable Robotics research community is to create robotic systems which are able to take advantage of modularity to allow novel capabilities. Some of the more commonly referenced potential advantages which might be possible with such systems include the ability to adapt to new tasks on demand, the ability to repair or replace damaged components and the ability to upgrade and change functionality programmaticly. Approximately a hundred systems have been proposed and prototyped since the early 1980's, with the motivating themes ranging from reconfigurable furniture [59] to systems dealing with reconfigurable space structures, e.g. [75], [56] and more recently [26] and [44], to the concept of programmable matter, i.e. the ability to basically create anything whatsoever [39]. The topics of discussion covered in this section include a brief summary of the history of the MSRR field, a look at some of the important topics of research in the

21

field including algorithmic developments and connector designs. Next, subsection 2.1.1 through subsection 2.1.3 take a deep look at the different algorithmic frameworks which have been developed to guide reconfiguration algorithms and hardware design. The following are a few terms which appear in the academic literature, which roughly mean the following:

- *Module:* The smallest discrete unit which fits into the modular architecture. These can be active (with electronics and actuators) or passive (provide structure and connections only).

- *Meta-Module:* Grouping of more than one module together to form a larger unit with enhanced capabilities. Often used to attempt to adapt modules to movement frameworks which are unachievable using single modules.

- *Connector:* The interface point where modules form and break connections with other modules. The design of simple and effective connectors is considered to be an unsolved challenge in the field of MSRR.

- *Movement Framework:* A model used to describe how MSRR modules move relative to each other. The most prevalent is the Sliding Cube Mode (SCM), but there are also the Expanding or Prismatic based model, in addition to the Pivoting Cube Model.

- *Configuration:* Particular grouping of modules which are connected through their modular connections. A configuration can usually be represented as a graph or tree structure.

- *Chain vs Lattice vs Hybrid Systems:* Chain systems are MSRR which have rotational joints, and are best represented as kinematic chains. Lattice Systems in contrast can be fully defined by a regular lattice. Hybrid systems implement characteristics of both chain and lattice morphologies.

The overarching research goal has been remarkably consistent since the early work in the 1980's. This goal is well summarized by Fukuda in 1988 [20] as, *"Such a system called the dynamically reconfigurable robotic system (DRRS), which can reorganize its*

shape and structure dynamically by employing limited available resources for a given task and strategic purpose." Since this early work, there have been many different systems built, and many more only imagined and simulated. Yim and many of the other prominent researchers in the field wrote this seminal survey article in 2007 [74], and there have been several surveys written since 2007 as well, including [16] and most recently [11] in 2017. A significant quantity of the research was funded by a DARPA grant [79], which sought to develop *"MesoParticles [which] communicate and interlock with their neighbors to create dynamic bulk structures with mechanical integrity"* and to *"imagine an amorphous material that can be programmed to instantly become a hammer, a wrench, or a screwdriver on demand. And then return to its initial form - so it can be reused."* This project funded many of the projects starting from 2008 and ending in 2010. Since then finding significant sources of funding for the MSRR community have been challenging.
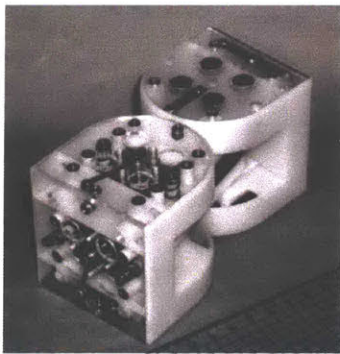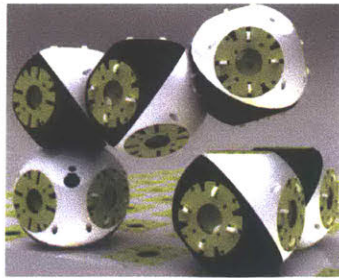
(a) M-TRAN module [42]   (b) Roombots system [59]   (c) SMORES system [15]

Figure 2-1: Examples of chain and hybrid MSRR systems, including the (a) M-TRAN system [42] developed beginning in 2002. (b) The Roombots system [59], which began development in 2010 (c) and the SMORES system [15] which began development in 2012.

Almost every proposed modular robotic system uses an entirely different type of connector, and developing a 'universal' connector remains a goal of the research community. Aside from the fundamental requirement of providing robust mechanical links, connectors have been used in the literature to enable inter-module communication [37, 67], to deliver power to modules and determine the presence and relative orientation of adjacent units. Many of the existing modular systems depend on complex, mechanically active connectors which require careful alignment [80, 58, 74, 73]. The M-Blocks use passive magnetic

connectors which automatically self-align. While these magnetic connectors may not be as strong as protruding mechanical latches found in other systems, they simplify reconfiguration movements. Continuing advancements in advanced connector design, such as solder-based connectors [43] may provide additional options for the 3D M-Blocks in the future to supplement the existing magnetic connections.

Most existing modular systems are also limited by the inability of the modules to move independently. Including the 3D M-Blocks, several systems do offer independent module movement, for example M^3Express [73] uses wheeled modules that can drive individually towards each other. Other systems, for example the SMORES [15], can either drive or inch along the ground to move, but are likely limited to movement on smooth surfaces due to very limited clearance between the wheels and the ground. However neither of these systems are designed to reconfigure according to any of the generalized reconfiguration movement models. Many of of the chain and hybrid systems are able to locomote with groups of modules, although often this requires a substantial number of modules to be effective. The Roombots [7] have demonstrated many interesting methods of locomotion, including moving with wheels, arms and legs, and the Atron [13] system has developed algorithms to control the gaits of legged systems which adapt to changes in the configuration while moving. While they cannot form legged structures the 3D M-Blocks are the only self-reconfigurable robots capable of implementing a simple movement model in three dimensions while also allowing independent module locomotion.

Modular self-reconfigurable robots are often characterized by their system topology: lattice, chain, or hybrid [74]. Most of the systems currently under development including U-Bots [80], Roombots [58], and SMORES [15] utilize a hybrid architecture. The fundamental distinction between hybrid or chain modules and strict lattice systems is that hybrid or chain modules have either fewer connector faces than lattice faces, or these connector faces can be located in off-lattice positions. Chain and hybrid systems are typically designed to self-reconfigure using complicated implementations which approximate one of the general movement frameworks, such as the Sliding Cube Model [17] or the Pivoting Cube Model [49]. Since the 3D M-Blocks system is strictly a lattice based system, the rest of this section will examine in detail the different lattice based movement frameworks and

the hardware systems which attempt to implement these frameworks.

2.1.1 Sliding Cube Model Systems

The Sliding Cube Model (SCM), as described in [9], and expanded upon in [17] is a conceptually simple framework, and has become the most prevalent model for algorithmic developments in the MSRR field. In the SCM any module or group of modules can slide relative to adjacent modules. There are many theoretical benefits of this system, mostly stemming from its simplicity. For example, a module can move into almost any empty space that has a direct line of sight to the outside world, therefore avoiding deadlocked configurations present in some of the other frameworks, as in the Pivoting Cube Model [61]. Additionally modules are assumed to be able to slide past each other, even when surrounded on multiple sides. In most versions of the SCM described in theoretical work, e.g. [19], modules are able to make convex corner transitions; this is referred to as the *strong* SCM. Alternatively the implementations of the SCM framework which do not allow convex corner transitions are termed the *weak* SCM. Recent work [29], has investigated algorithms for 3D reconfiguration according to the weak SCM. There have been several systems attempting to implement various versions of the SCM in physical hardware, as seen in Table 2.1 and Figure 2-2, however none of them are able to implement the 3D version of either the strong or weak SCM with the effects of gravity.

Table 2.1: Table listing several of the MSRR systems which attempt to implement the Sliding Cube Model. Many different approaches to providing movement are represented in this sample of systems, including electromagnetic interactions, adhesives, and rack and pinion mechanical connections. In this context, system capabilities labeled as *weak* means that there are no concave corner traversal moves allowed, while *strong* systems do allow these moves.

System Name	Year	Capabilities	Notes
Square Modules	2001	2D Strong	[12]
EM Cubes	2007	2D Weak	[2]
Sticky Bricks	2007	2D Weak	[54]
CHOBIE II	2008	2D Strong	[62, 32, 63]
Helical Magnetic Cubes	2017	3D Weak	[64]
Conveyor	2013	2D Weak	[46]

(a) CHOBIE II [62]   (b) Helical Magnetic [64]   (c) EM-Cubes [2]

(d) Square modules [12]   (e) Conveyor Robots [46]   (f) Sticky Bricks [54]
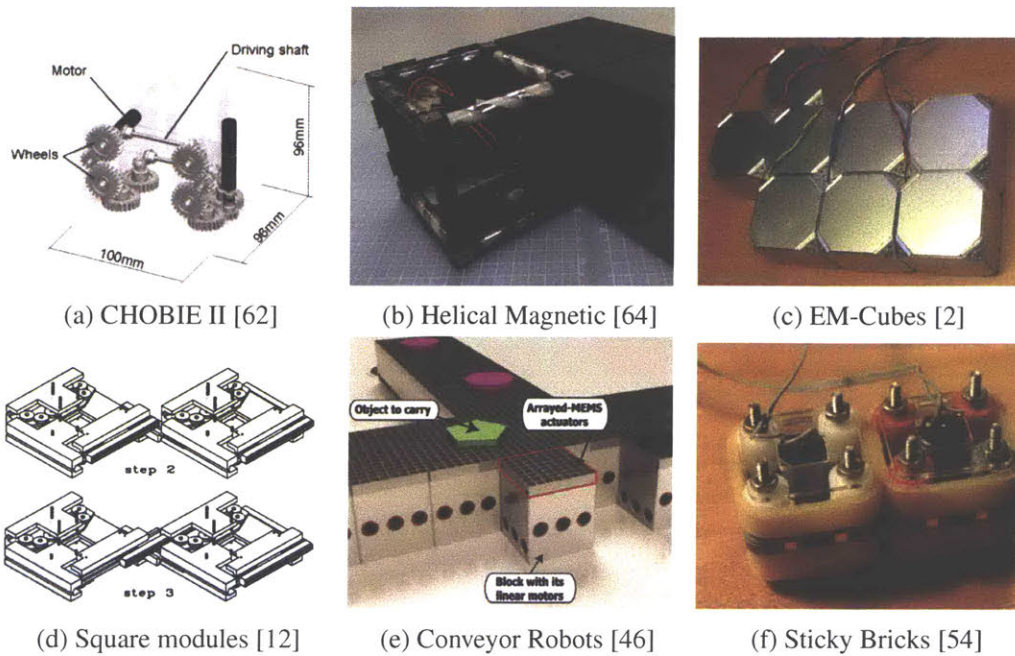
Figure 2-2: Select MSRR Systems designed to implement the Sliding Cube Model. Including (a) CHOBIE II [62] which uses a rack and pinion (b) Helical Magnetic Robots [64] utilizing magnetic screws (c) EM-Cubes [2] which use electromagnets (d) Square modules in [12] (e) Conveyor Robots [46] which also use electromagnets, and (f) Sticky Bricks [54] which use adhesive belts.

One of the most challenging issues encountered with creating hardware which implements the Sliding Cube Model is the problem of corner traversal movements. If the assumption that the modules fill the entirety of the space of a cube, and don't extend past this unit cubic volume, then when making a convex corner traversal the module would be supported by an infinitely small line at some point during the movement. Any actuation method that primarily uses the faces to generate attractive and shear forces, e.g. all of the systems labeled *weak* in Table 2.1, will not be able to perform these movements. If the requirement that each module doesn't extend beyond its cubic volume is relaxed, then solutions can be designed that allow for the concave corner transition. However the only systems which attempt to implement the strong SCM use extending rack and pinion mechanisms which are mechanically complex. Both of these systems, including CHOBIE II [62], and the Square Modules in [12] are limited to 2-dimensional movements. While it might be possible to create a 3D version of modules with extending racks and pinions, significant challenges

26

involving the alignment and gender of the connectors would need to be addressed.

Attempts to implement the weak SCM have been more numerous, and illustrate the diversity of actuation designs in the MSRR field. For example the Sticky Bricks [54] move using a rolling adhesive patch, almost like an adhesive treadmill attached to each face. However this systems has not yet been extended to three dimensions, and would likely face design challenges if this is attempted. Several systems use electromagnets in order to shift modules relative to each other, including the EM Cubes in 2008 [2], and the Conveyor in 2013 [46]. However, these systems like many of the others are limited to two dimensions. While many of these actuation strategies, including the electromagnetic method, could potentially be extended to three dimensions, there have not been many attempts to do so. Additional systems use magnetic forces, including the 2017 [64] work using helically magnetized cylinders to slide modules along as if they were attached together with screws. While this method is promising, the current hardware cannot lift a module past the force of gravity, therefore greatly limiting its practical capabilities. Additionally, there are systems which are able to self-reconfigure in three dimensions [35, 34], but these systems all diverge from the simplicity offered by the sliding and pivoting cube models. There are no preexisting three dimensional hardware systems which are able to reconfigure in a manner that directly mimics the strong SCM. There is still continuing hardware and theoretical work in this area; recent research [27] has produced a provably correct self-reconfiguration algorithm for two dimensional systems based on the SCM.

2.1.2 Expanding Cube Model Systems

The expanding, (a.k.a. Prismatic, or Crystalline) cube model (ECM) is an alternative movement framework which also allows for general 3D reconfiguration [50], although this model is not as theoretically capable as the SCM. Instead of sliding past each other as in the SCM, each connector face on the lattice is able to linearly expand by at least half of a lattice length. This allows modules to move in an almost inchworm-like method to new lattice positions. One of the main theoretical disadvantages of this framework is that there is no way to perform concave corner traversals without the help of adjacent modules.

(a) Telecubes [28]   (b) Crystalline Modules [51]
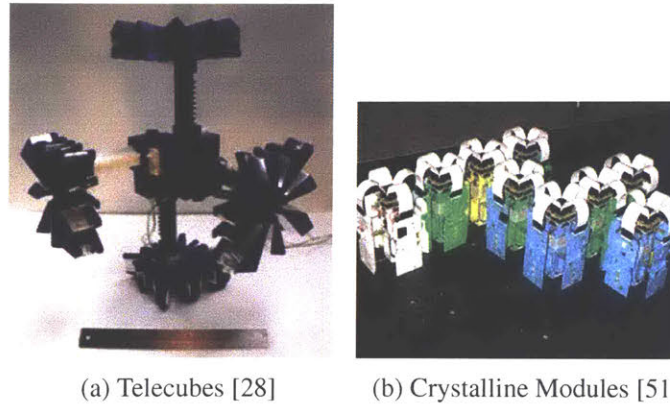
Figure 2-3: Selection of modular robots which move according to the Expanding Cube Model, (a) The Telecube Modules from Goldstein et al. [28] and (b) The Crystalline Modules [51].

The expanding cube model is described in more detail in the works of Butler and Rus [10] in 2003 and in 2011 by Aloupis [1]. Although there are not that many hardware systems employing the ECM, there has been continued algorithmic development, including [57]. There is also the possibility of using meta-modules to emulate the ECM, which provides interesting avenues for future research, as algorithmic based on the ECM framework could then be extended to hybrid or chain systems.

Table 2.2: Comparison of MSRR Systems based on the Expanding, or Prismatic cube model. The Prismatic Cubes from 2009 appear to be able to implement the full 3D ECM model, but there seems to only have been a limited number of modules constructed.

System Name	Year	Capabilities	Notes
Crystalline Atoms	2001	2D	[51, 8]
Telecubes	2002	3D	[60, 28]
Prismatic Cubes	2009	3D	[69]

From a mechanical standpoint, there are many challenges to creating modules which follow the expanding cube model. One challenge is the necessity of including six linear actuators and linear bearing surfaces, in addition to six connectors. Implementing linear motion is difficult, and in general is more challenging to fabricate and control than rotating mechanisms. Also, during each move the system has to support the whole weight of the structure on a cantilevered arm. If multiple modules are to move together there is a serious risk of over-constraining the linear motion, which could prevent motion altogether,

28

essentially causing the system to jam. Additionally none of the ECM based systems have a mechanism for individual modules to move in a non-lattice environment.

2.1.3 Other Lattice Systems

While this review excludes chain-based systems, there are a few classes of modules which also have a full set of lattice connections, but provide reconfiguration in different ways, as shown in Table 2.3. There are several examples of systems which achieve shape formation through disassembly, including Miche [23] and the Robot Pebbles [24, 25]. These systems contain only active modular connectors and rely on external forces in order to create structures, almost like a sculpture which can sculpt itself.

Additionally there are several systems which use a stochastic fluid in addition to active connectors in essence to selectively grow desired structures. These systems include work by White [72] and Tolley [66] at the Creative Machines Laboratory. The advantage of using stochastic fluids is that there is no need for the complex actuators used by most of the other systems. It is interesting to note that most of the biological based systems which are able to reconfigure modular building blocks e.g. DNA and protein production, use stochastic fluid based mechanisms, which hints that this approach might be a promising area for future research. Additional systems have been designed to create 2D structures of cubic lattice elements on the surface of liquids, including interlocking robotic boat tiles [52], in addition to proposed flying systems including the Distributed Flight Array [45], which uses hexagonal modules to assemble 2D flying structures.

Table 2.3: Listing of other lattice based MSRR modules.

System Name	Year	Capabilities	Notes
Stochastic 3D Assembly	2004	3D fluid	[66]
Miche	2006	2D Disassembly	[23]
Distributed Flight Array	2010	2D Fluid	[45]
Robot Pebbles	2012	2D Disassembly	[24]
Modular Boats	2017	2D Fluid	[52]

29

<div style="text-align:center">(a)   (b)   (c)</div>
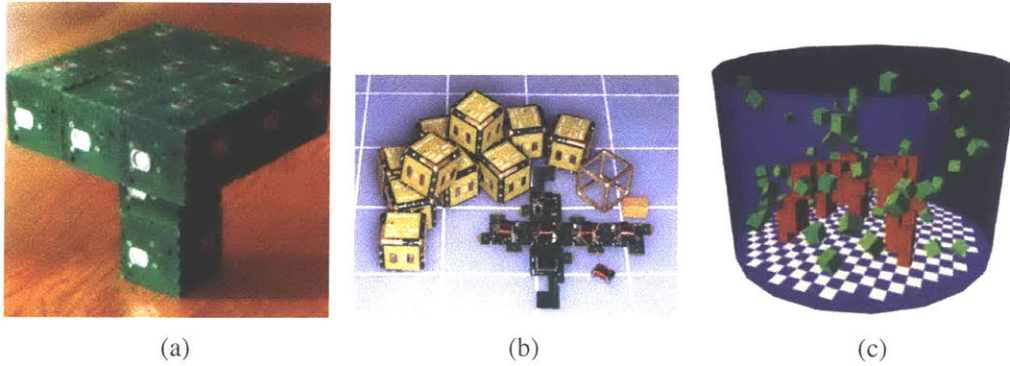
Figure 2-4: Additional lattice based MSRR systems, including self-disassembly and stochastic systems (a) Miche System [23] (b) Robot Pebbles [24] and (c) 3D Stochastic Cubes [66].

2.1.4 Pivoting Based Systems

While the Sliding Cube Model has been the most prevalent abstraction for lattice based reconfiguration, there has also been significant development of systems which utilize pivoting motions. In general, pivoting motions are mechanically simpler to implement and control than sliding motions, and there are many systems which implement at least some degree of pivoting in pursuit of reconfiguration. Figure 2-5 and Table 2.4 give an overview of some of the previous work involving systems implementing pivoting motions.

Table 2.4: Comparison of MSRR systems utilizing pivoting motions

System Name	Year	Capabilities	Notes
Fracta	1997	2D	[77]
X-Bot	2007	2D	[70]
CMU Planar Catoms	2007	2D	[30]
Octobot	2008	2D	[55]
M-Blocks	2008	3D	[49]
Flux-Pinned Spacecraft	2008	2D	[56]
3D Pivoting Tetrahedrons	2011	3D	[72]
Reconfigurable Space Structure	2017	3D	[44] - Design Only

One of the challenging practical implementation elements of pivoting systems has been forming hinges between modules. These hinges need to be able to fulfill a significant list of requirements, including:

<div style="text-align:center">30</div>

(a) X-Bot [71]   (b) Flux-pinning [56]

(c) Reconfigurable Space [44]   (d) Planar Catoms [30]
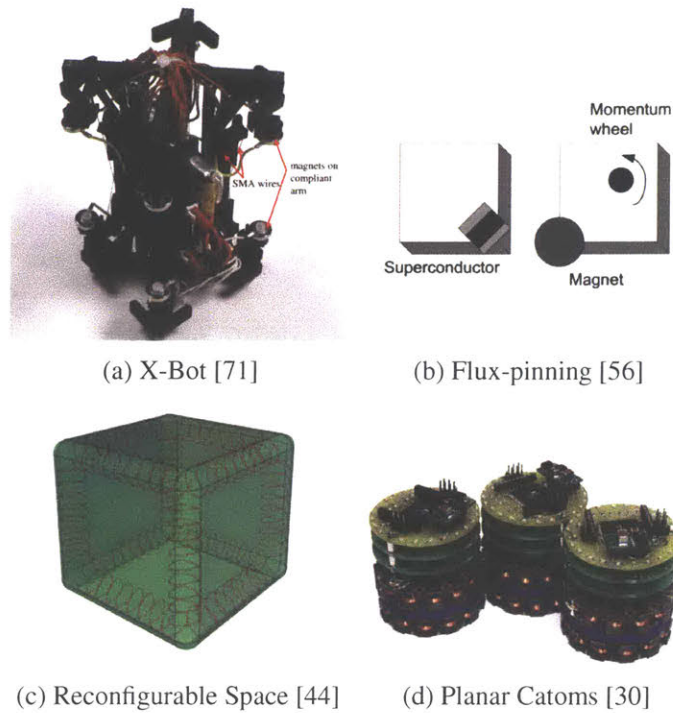
Figure 2-5: Select MSRR Systems which implement rotating, or pivoting reconfiguration motions. These include (a) X-Bots from White et al [71] (b) Reconfigurable spacecraft using flux-pinning, EM Reconfigurable Space Structure [44], and (d) Planar Catoms [30] from CMU.

1. Hinges must be able to be engaged and disengaged under the correct circumstances.

2. Hinges must be present on all 12 edges of a cubic module, and be able to connect in any 3D orientation (i.e. they must be non-gendered).

3. Be strong enough to remain connected while experiencing the forces and torques required for reconfiguring.

Often the first idea to create hinges is to use some form of magnetic attraction. Systems using hinges based on magnetic interactions range from superconducting magnets [56] to electromagnets [44], [30], [55] to different configurations of actuated permanent magnets [70] to combinations of permanent and electromagnets, as in the Fracta [77]. There are also systems which use physical connecting hinges, such as [76], which even proposed a full 3D system with octahedral modules. The hinges introduced in the 3D M-Blocks [49],

extend upon this previous work since they allow for a full 3D system using passive me-
chanical re-alignment to allow un-gendered hinges.

Once the hinges are implemented, an actuator needs to provide motion around the
hinge. One system [56] proposed the use of reaction wheels to rotate the modules about
superconducting hinges as shown in Figure 2-5 (b), but this sytem was never developed into
a full 3D system. The X-Bot system [70] and [3] used external forces to generate torques
due to inertia from a moving table to rotate modules about hinges which were actuated with
shape memory alloys. Many of the systems which use electromagnets including the CMU
Catoms [30], and the Octobot [55], also use the repulsive forces from the electromagnets to
induce rotation. However electro-magnets are heavy, have limited forces, and are require
significant circuitry and continuous power to operate. One promising potential avenue to
provide both locomotion and hinges is through the use of electro-permanent magnets, as
described in [40], and used as face to face connectors in SMORES [67]. However EPM's
also face many of the same challenges as electromagnets. Additionally, EPM's face an even
more dramatic force drop-off relative to distance as compared with electromagnets, and the
difficulty of high cost and difficult sourcing for the necessary components.

2.2   Inertial Actuation

Most robots generate movement by directly interacting with the environment by applying
forces to it, e.g. wheels or legs pushing off from the ground or other entities. However it is
also possible to generate relative movement by manipulating internal masses and angular
momentum. By taking advantage of the laws of conservation of angular momentum, large
torques can be generated using several different designs including reaction wheels and con-
trol moment gyroscopes. Spacecraft have pioneered the use of angular momentum based
actuators since they have nothing to "push" against in the vacuum of space. The use of
inertial actuators has spread to terrestrial robots in recent years, likely due to the simplicity,
robustness and fine-tuned control offered by these systems. This section will first provide
a quick overview of reaction wheels and control moment gyroscopes, before concluding
with a brief review of some of the robotic systems which utilize inertial actuation.

32

2.2.1 Inertial Actuation Overview

While the concept of linear momentum is relatively easy to understand, the concept of the conservation angular momentum can be more difficult to fully understand. In three dimensions the deceptively simple equation 2.1 describes the vector relationship between the sum of external torques and the time rate of change of the angular momentum vector.

$$\sum \vec{T_{ext}} = \frac{d}{dt}\vec{H}_o \tag{2.1}$$

The key to understanding equation 2.1 is to focus on the fact that all of the quantities are vectors. This is why gyroscopes, or holding a bicycle wheel while sitting in a chair, can produce counterintuitive results. A flywheel is simply a element which stores angular momentum by spinning, with the angular momentum vector parallel to the axis of rotation, as seen in Figure 2-6. There are two main methods of generating torques from flywheels as demonstrated in Figure 2-6, reaction wheel actuators generate torques by changing the angular velocity of the flywheel. This generates a torque about the axis of the flywheel, either positive or negative based on the change in magnitude of the angular momentum vector. Alternatively torques can be generated by changing the direction of an angular momentum vector; these actuators are commonly called control moment gyroscopes.

(a) Reaction wheel   (b) Control moment Gyroscope
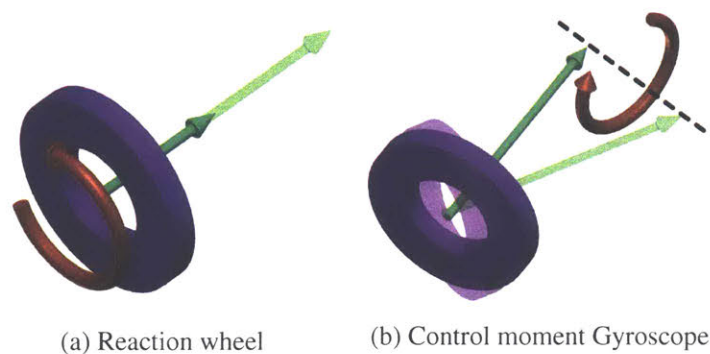
Figure 2-6: Illustration of two common methods of creating inertial forces including (a) reaction wheel, and (b) control Moment gyroscope. The *orange* arrows indicate the torque generated due to the change in the angular momentum vector, with the *solid green* arrow representing the final angular momentum vector, and the *transparent green* arrow representing the initial vector.

Reaction wheels are the simplest type of inertial actuator. A reaction wheel, as shown in Figure 2-6 (a) spins a flywheel, usually with an electric motor integrated into the inside of the flywheel, in order to store and transfer angular momentum. Assuming the direction of the plane of rotation doesn't change, a reaction wheel generates torque only when its angular velocity is changing. This leads to one of the reaction wheels' most serious limitations, which is a saturation of torque in a particular direction due to reaching a maximum speed of a particular flywheel and motor combination. The physical limits that set this maximum speed are complicated; depending on the material, bearings, motor and other factors and are explored in some depth in [6]. The main takeaway is that reaction wheels are simple to implement mechanically, are very robust, but cannot generate torque in the same direction continuously.

Control Moment Gyroscopes (CMG) in contrast generate torque from changing the direction of an angular momentum vector, usually but not always while holding the magnitude (i.e. the angular velocity) constant. These actuators are used extensively in the space industry, but they are relatively difficult to fabricate and control, and are described in more detail in works such as [65], and [68]. The primary advantage of a CMG is that it does not have the saturation problem inherent with reaction wheels, and when used in combination with multiple CMG's can generate torques in arbitrary directions for arbitrary lengths of time. The design of CMG's are complicated by the need for stages, i.e. gimbals, which hold the flywheel and motor, which need to rotate relative to one another. The mechanical design of these gimbals becomes complicated due to the requirements for high stiffness over a large area in a constrained space. This difficulty is magnified considerably when the CMG contains more than one gimbal. Additionally systems which have multiple gimbals can experience a phenomenon called gimbal lock where the separate gimbals kinematically 'collapse' and reduce the controllable degree of freedom.

2.2.2   Inertial Actuation in Robotics

There are several interesting robotic systems which utilize inertial forces to provide movement. While the bulk of the work involving inertial actuators are in spacecraft, there have

been several systems, mostly research platforms, which use reaction wheels for motion, and a few which use CMGs. While there are few systems which have practical uses beyond research, there also has been increasing interest in using reaction wheel powered robotic rovers to explore low-gravity locations such as asteroids.

| (a) Cubli [22] | (b) Hedgehog [47] | (c) Spherical Robot [53] |
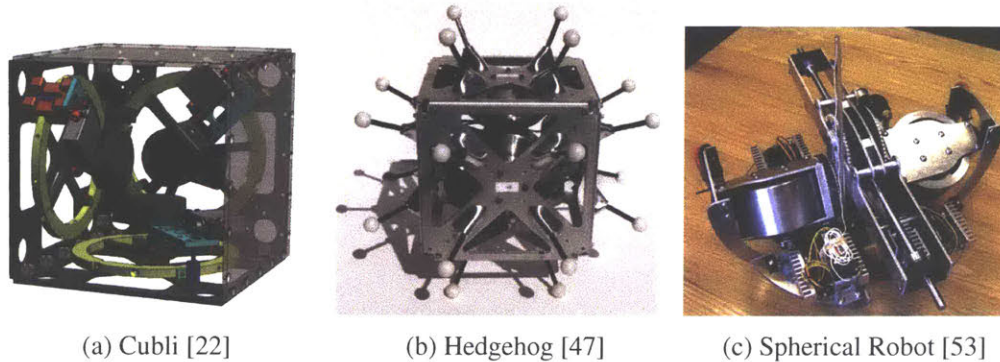
Figure 2-7: Select robotic systems using inertial actuation, including systems which use primarily reaction-wheel actuators, (a) Cubli [22] (b) Hedgehog Rover [47], and one which uses CMG's for locomotion: (c) Spherical Robot [53].

The Cubli, [22, 21], developed at ETH Zurich and Cubli-inspired designs like the *Nonlinear Mechatronic Cube* from Chalmers University [5] are a groundbreaking series of robots which use reaction wheels combined with a quick acting brake in order to provide locomotion to a cubic module. The Cubli was preceded by many related works which use a reaction wheel to attempt to balance one or two degrees of freedom inverted pendulums, e.g. [41], often used as educational exercises in implementing control theory. The Cubli is a 150 *mm* side length cube, which has three orthogonal reaction wheel actuators which can generate short spikes of torque in order to roll the device onto its corner. The brake mechanism, as described in [22] uses a servo to bring a piece of material in contact with an extrusion extending from the flywheel, somewhat similar to jamming a stick in the spokes of a bicycle. The Cubli is able to generate enough torque to stand up on its corner, and to roll about an edge, but it is not shown counteracting any additional torques besides its own inertia and gravity. In contrast the 3D M-Blocks modules have to overcome the significant magnetic torques of adjacent modules, which is illustrated in Figure 4-9, which are several orders of magnitude more than the torque due to gravity alone. Also the Cubli is intended to be a platform to test control algorithms, and does not attempt to interact or connect with

35

other robots.

One additional class of inertially actuated robots are spherical robots. These robots are generally fully enclosed plastic spheres which have some internal mechanism to generate rolling or inertial forces. Some robots, including the Sphero [38], generate movement by basically rolling an unbalanced mass inside of a sphere like a hamster wheel. There are several other robots which use reaction wheels, and even one which uses a control moment gyroscope. The spherical robot developed by Schroll in [53], and shown in Figure 2-7 uses two CMG's to allow it to move over challenging terrain.

In addition to earth bound robotics, there have been several robots created and proposed with the goal of exploring celestial bodies including asteroids. The Japan Space Agency created the Minerva Rover [78] in 2006 which was intended to explore asteroids including. The Hedgehog robot [31] presented in 2014 has a similar goal, and uses the same triple flywheel configuration as the Cubli. These designs are promising for locomotion in a low gravity environment since the use of reaction wheels allows omni-directional controlled motion (i.e. they can't be placed 'upside down' like a wheeled rover can) and they can be completely sealed from the dangers present in these environments including dust and debris kicked up by their own movements.

Chapter 3

3D Pivoting Cube Model

This chapter introduces a movement framework called the 3D Pivoting Cube Model (PCM). This framework builds off of existing work to define a set of rules for modular robots to reconfigure on a general cubic lattice in three dimensions. Section 3.1 introduces the rules and assumptions of the PCM, and briefly discuss algorithmic developments and off-lattice movements of modules. Section 3.2 provides an initial analysis of the dynamics of modules moving on a lattice according to the PCM, assuming some practical considerations involving the existing hardware.

3.1   3D Pivoting Cube Model Definition

The Sliding Cube Model (SCM) 2.1.1 is one of the more prevalent algorithmic frameworks that has been developed for modeling the motions of lattice based self-reconfiguring modular robots. However it is difficult to implement this model in hardware due to the practical challenge of implementing concave (i.e. around a corner) moves. To overcome the physical implementation issues of the sliding cube model and to utilize the favorable traits of the 3D M-Block hardware presented in Section 4, this section presents the *3D Pivoting Cube Model* (PCM). This model expands upon existing theoretical models presented in previous works, including [4], and those covered in Section 2.1.4 to create a clear set of guidelines for lattice locomotion of modular systems. In the PCM, cubic modules locomote by pivoting about their edges, in effect rolling from one position to the next. This section is Adapted

from the work in [49].

The PCM makes the following assumptions about the modules involved:

1. Each cubic module has a magnetic based hinge on each of its 12 edges, and there is a radius, or chamfer, on this edge.

2. No component of the module permanently extends beyond the boundary of the cubic module.

3. Each of the six faces holds a connector to connect to other faces.

This list of requirements leads to several notable results that are relevant to the development of algorithms to reconfigure structures.

- While already assumed by other models [4], the modules involved in pivoting motions sweep out a volume that must not intersect other modules. Figure 3-1 (a) demonstrates this requirement.

- Stable lattice configurations must have modules connected via their faces, not their edges. (This is in contrast to other models [4].) Figure 3-1 (b) illustrates this requirement.

- Modules involved in pivoting motions must be able to slide past stationary modules in adjacent planes. This allows modules in the different initial slices to move independently, and is shown in Figure 3-1 (c).

- Multiple modules can move as a connected unit, but they must all share a single axis of rotation, as shown in Figure 3-2.

Modules, or groups of modules, moving according to these rules are able to execute a range of motions including concave transitions, convex transitions, and linear translations. The requirement that modules don't extend past the cubic module adds complexity to the design of the modules, but simplifies the control algorithms, allowing independence between different 'layers' of a structure. When operating on a lattice, groups of modules

| (a) | (b) | (c) |
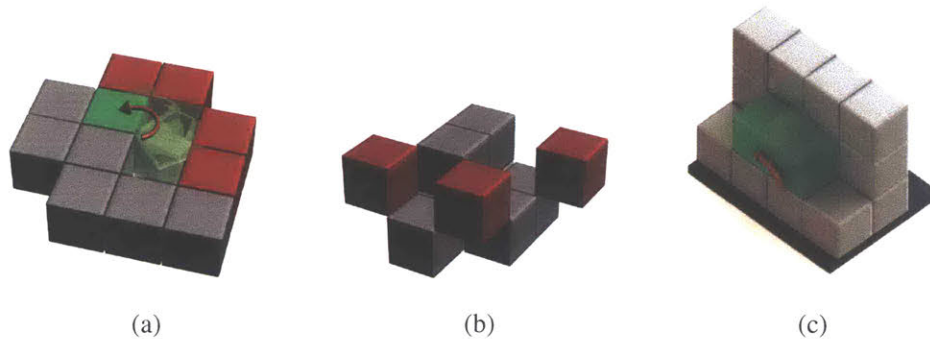
Figure 3-1: This figure illustrates several of the characteristics of the PCM. Moving cubes sweep out a volume that must be free from other cubes in order to allow motions (a). Although cube edges bond to each other, due to the rounded edge geometry, any cube attached only through edge bonds (shown in red) is not part of the regular lattice configuration (b). Faces have no protruding elements which allows cubes to slide past each other, although in practice friction can be significant (c).

that share the same pivot axis are able to coordinate their actuators in order to move together. Not only does this increase the stability of the motion due to longer pivots as in Figure 3-2(a), but it also decreases planning complexity when attempting to relocate multiple modules on a lattice.

Different physical implementations of this model will have varying forces and dynamic constraints, and some moves that are kinematically possible might be very difficult in practice. Section 3.2 begins to investigate the dynamics of this model applied to the 3D M-Blocks hardware by introducing include mass, inertia, gravity, and magnetic forces. However this model is rudimentary and makes several significant simplifications including that the modules are rigid bodies and that the pivot axes do not slip.

3.1.1 PCM Reconfiguration Algorithms

While the specifics of the movements allowed in the PCM differ from those of the SCM, pivoting still allows generalized reconfiguration. Benbernou [4] presents a 2D algorithm that reconfigures a set of pivoting 2D square tiles to transition from any initial state to almost any goal configuration, although this seems to allow weakly-connected tiles, which are not allowed in the PCM. The algorithm works by sequentially rotating all modules around the boundary of the structure in a clock-wise fashion until they form a line. Starting

<div align="center">(a)   (b)   (c)</div>
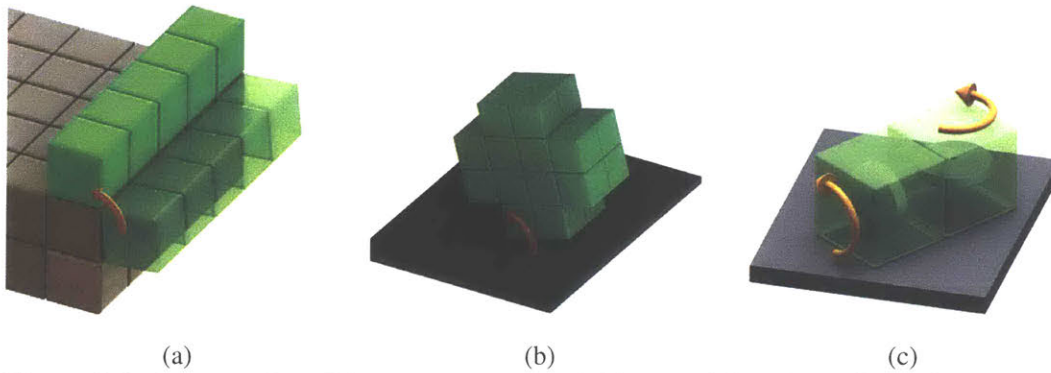
Figure 3-2: Groups of modules can move as a rigid assemblies. Two-dimensional movements can be extended along the pivoting axis (a). Modules can aggregate and roll as an assembly (b). Two 3D M-Blocks with orthogonal inertial actuators can form an easily controllable meta-module (c).

from this line, the modules can execute similar inverse motions to reach some goal configuration. Recent work by Sung et al. [61] proposes expanding Benbernou's algorithm to operate in 3D by slicing the initial configuration of modules into a set of parallel planes. The algorithm is executed on each plane in order to condense the 3D structure into a single plane. Then, the algorithm is applied a final time in an orthogonal plane to achieve the canonical line configuration (from which the goal configuration can constructed). While this algorithm does not work for all input structures (some specific sub-configurations are not allowed) it provides the foundation for applying practical algorithms to the 3D Pivoting Cube Model in the future.

3.1.2 Additional Locomotion Methods

Assemblies of modules are able to move together in the environment by first reconfiguring in order to approximate a wheel or sphere, as shown in Figure 3-2(b), and then simultaneously applying their inertial actuators. An additional type of group movement involves small groups forming meta-modules, as shown in Figure 3-2(c), which can more precisely control their trajectories. The modules can be oriented such that their actuators are aligned in orthogonal planes allowing control over additional degrees of freedom. When a disjoint group of modules is self-assembling, these meta-modules can serve as intermediate

assemblies to increase the speed of the aggregation.

In particular, a disjoint set of modules can locomote over open ground to coalesce at a centralized point and then proceed to form an arbitrary structure. In order for modular robots to realize self-assembly and robust operation, the unit modules need to be both self-contained and independently mobile. Although researchers have produced modular systems in which the modules can locomote independently, these systems are limited to laboratory environments [67, 36]. In contrast, the 3D M-Blocks are independently mobile, and they show an ability to move through difficult environments. Although they only have a single actuator, they can exhibit several motions including rolling, spinning in place, and jumping over obstacles up to twice their height.

This diverse set of motion primitives enables novel motion algorithms. One method that is used drive 3D M-Blocks towards a specific goal is to implement a bimodal behavior. When the module's actuator is aligned with the goal location, the actuator is used to apply a moderate amount of torque that causes controlled rotation toward the goal. When the module is not aligned with the goal, the module is stochastically reoriented using a short pulse of torque which causes random movement. A group of disjoint 3D M-Blocks executing this behavior can self-assemble into a lattice structure.

3.2 Dynamics for the Pivoting Model

While the Pivoting Cube Model clarifies how the modules move kinematically, the dynamics involved with pivoting motions on real hardware systems require more analysis. This section will set up, but not attempt to solve, the differential equation of motion about the pivot axis which can provide insight into the actuator requirements for design of a hardware system. While this model, as illustrated in Figure 3-3 does not attempt to solve this equation as a function of time, it provides the foundation for applying these techniques in future work. Because inertially generated torques can be considered as pure moments, the applied torques from several connected modules can be superimposed and applied en masse about the assembly's pivot axis. If the single module in Figure 3-3 is viewed as a generalized set of modules moving as a rigid unit, one can construct a torque balance equation for the

41

assembly, by just adding the torques together and remembering to apply the parallel axis theorem to correctly calculate the moment of inertia about the pivot axis. This analysis makes the following assumptions about the motion of modules:

1. The hinge is exactly at the corner of the cube (An approximation of the 3D M-Block hardware) and is frictionless, and remains connected at all times.

2. All of the forces and torques occur only in a single plane perpendicular to the axis of the reaction wheel, and are limited to those torques from (1) the actuator, (2) gravity, and (3) the interaction between matching pairs of hinge magnets.

3. The module and the flywheel are rigid bodies, i.e. no flexing or deformation.

The torques and positions are illustrated in Figure 3-3, and the following are the variables used in this analysis of the system:

- θ: The angle between a rotating module and its original orientation.

- $\frac{d^2\theta}{dt^2}$: The angular acceleration of the angle θ.

- I_{module}: The moment of inertia of the module, including the flywheel.

- $F_m^{(k)}(\theta)$: The force between the k th pair of magnets as a function of theta.

- $r^{(k)}$: The vector from the pivot axis to the k th magnet pair.

- r_{cg}: The vector from the pivot point to the center of gravity of the module.

- m_{module}: Mass of the module, or group of modules.

- $T_{ia}(t)$: The torque applied to the module's frame from the inertial actuator as a function of time.

$$\frac{d^2\theta}{dt^2} = \frac{T_{ia}(t) - m_{module} \cdot g \cdot cos(\theta) \cdot |r_{cg}| - \sum_k F_m^{(k)}(\theta) \cdot r^{(k)}}{(I_{module} + m_{module} \cdot (r_{cg})^2)} \tag{3.1}$$

42
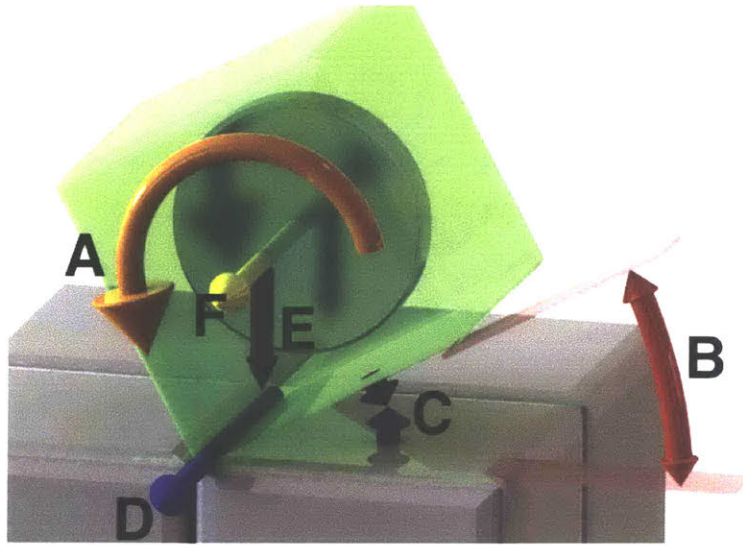
Figure 3-3: This figure is an illustration of the various significant elements in the dynamics of a pivoting motion as captured in Equation 3.1. When a torque (A) caused by the inertial actuator (*grey disk*) about an axis (F) causes the module to pivot through an angle θ (B) about a different axis (D), the modules experience additional forces: downward force due to gravity (E) and magnetic force from magnetic interactions (C).

Pivoting moves are dynamic in the sense that the motion is not directly controlled by the robot, as in a servo or a robot arm moving, instead coming from a torque generated inertially, therefore traditional position control loops utilized by many robots cannot be directly applied. What Equation 3.1 essentially reduces to is that if the torque applied by the inertial actuator can overcome the sum of the magnetic and gravitational torque, then it will break free and begin to start rotating about the pivot axis. In order to solve for the motion, Equation 3.1 would have to be analytically integrated, or more likely solved numerically. However an analysis of the torque balance, or the top half of the right side of Equation 3.1, can be useful in determining the torque required by the inertial actuator.

While not explicitly stated in the equation, θ is a function of time. Additionally the model ignores sliding friction which would be subtracted from the numerator of the right-hand side (thereby resisting the torque of the actuators) which will be highly dependent on the configuration of modules in adjacent planes. The basic message of the equation is that one should aim to maximize the actuator torques while minimizing the mass and inertia. While decreasing the magnetic bonding strengths would lead to lower actuator

torque requirements, those same magnetic forces are used to maintain the magnetic hinges and the system's structural integrity. Obtaining the correct balance between the hinge force and the bonding force is an area that would be interesting to investigate further.

Figure 3-4 shows the balance of torques plotted for a concave corner move fighting against gravity. In this figure, the magnetic torque is estimated from a 2nd order exponential fit to the experimentally determined force versus distance characteristics for the particular edge magnets used in the 3D M-Blocks. This plot shows the dominance of the magnetic torques at the beginning of the movement, being about a factor of 20 more higher than the gravitational torque. Once the module has rotated through an angle of about 30 degrees, the torques from gravity and the magnets are equal, this is due to the quick drop off of magnetic forces versus distance. The optimal design for the torque profile from the inertial actuator would be to ramp up to a torque higher than the initial maximum torque as quickly as possible, and then apply a lower controlled torque to efficiently rotate the module until theta reaches the point where the torques become negative.
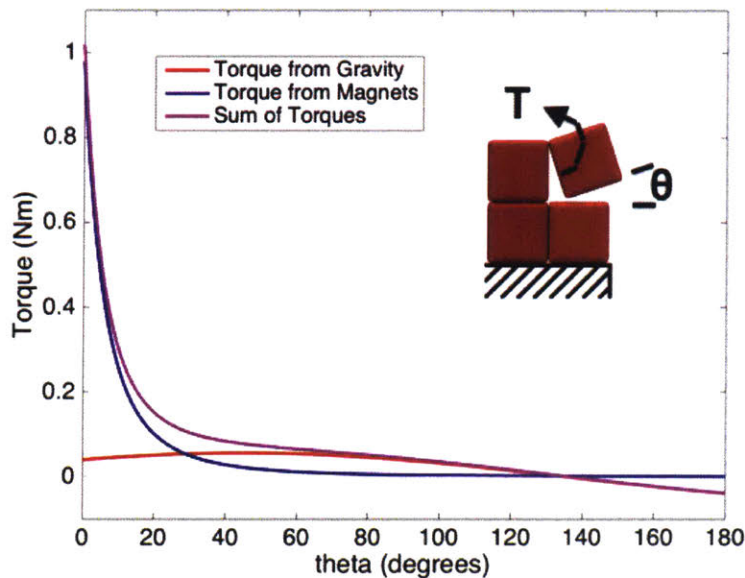
Figure 3-4: Graph of simulated torques experienced during motion. This graph adds the calculated torque due to gravity (*red line*) with the estimated magnetic torque (*red line*). It can be noticed that the magnetic torque is initially very significant, but drops quickly with increasing angular distance, while as expected the magnetic torque is a maximum at $\theta = 45$ *degrees*. The torque from the magnets on the face where the new connection is formed is omitted from the plot.

44

Chapter 4

System Design

This chapter covers the design of various subsystems contained in each 3D M-Blocks module. The first section introduces the functional requirements guiding the design and provides a basic time-line of development and an overview of module characteristics. The next section, Section 4.2, covers the development of the core assembly structure of the robot, i.e. the body which holds the inertial actuator and the electronics. Next, Section 4.3 covers the design of the inertial actuator which generates the torques required to implement locomotion and lattice reconfigurations. The next section covers the design of the frame structure which holds the core assembly, and provides the face connectors and magnetic hinges necessary for lattice reconfiguration. Section 4.5 covers the design of the system which switches the plane of the inertial actuator in order to allow motion in three mutually orthogonal planes. Finally section 4.6 covers the design of the electrical system in each 3D M-Block module. Additionally Appendix A includes a mechanical parts list in addition to electrical schematics for several of the circuit boards comprising the electronics system.

4.1 M-Blocks Design Overview

The goal of designing the hardware for the 3D M-Blocks is do investigate the challenges and evaluate potential solutions for the problem of creating modular robots which move by pivoting through inertial actuation on a cubic lattice. The following six functional requirements are the goals guiding the development of the 3D M-Blocks hardware. The modules

45

must:

1. Be able to generate enough inertial torque to overcome the combination of torques due to friction, gravity and magnetic bonding both clockwise and counter-clockwise in three mutually orthogonal planes.

2. Contain non-gendered magnetic hinges on all 12 edges of a cubic frame.

3. Be fully self-contained, including all mechanical and electrical elements, including an energy source and wireless communication capabilities.

4. Be able to sense immediate surroundings to determine select environmental stimuli in addition to sensing adjacent modules.

5. Be mechanically reliable and robust to repeated impacts.

6. Minimize the mass and moment of inertia of the modules, while maximizing the inertia of the flywheel inside the inertial actuator.
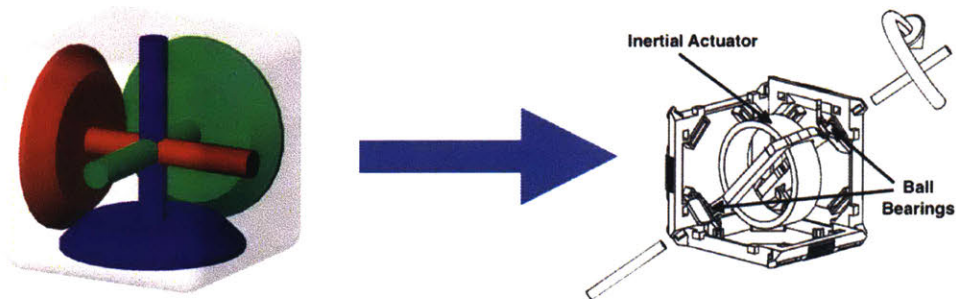
Figure 4-1: This Figure illustrates the significant design decision to move from three mutually orthogonal face-mounted flywheels, as in the Cubli [21], to a novel design including a single large flywheel which is able to move into three discrete positions corresponding with each of the three orthogonal planes of a cubic lattice. This design allows for maximizing the moment of inertia of the flywheel. This tends to increase the torque from the inertial actuator, while offering the simplicity of only a single additional rotating axis. In addition it is possible to have significant surface area on the flywheel to minimize the pressure in the flexible braking element of the inertial actuator.

The design which has been prototyped to meet these requirements is called the 3D M-Blocks, which consists of three primary mechanical assemblies: a frame (1) which holds the core assembly (2) which in turn supports the flywheel (3) as seen in Figure 4-2.
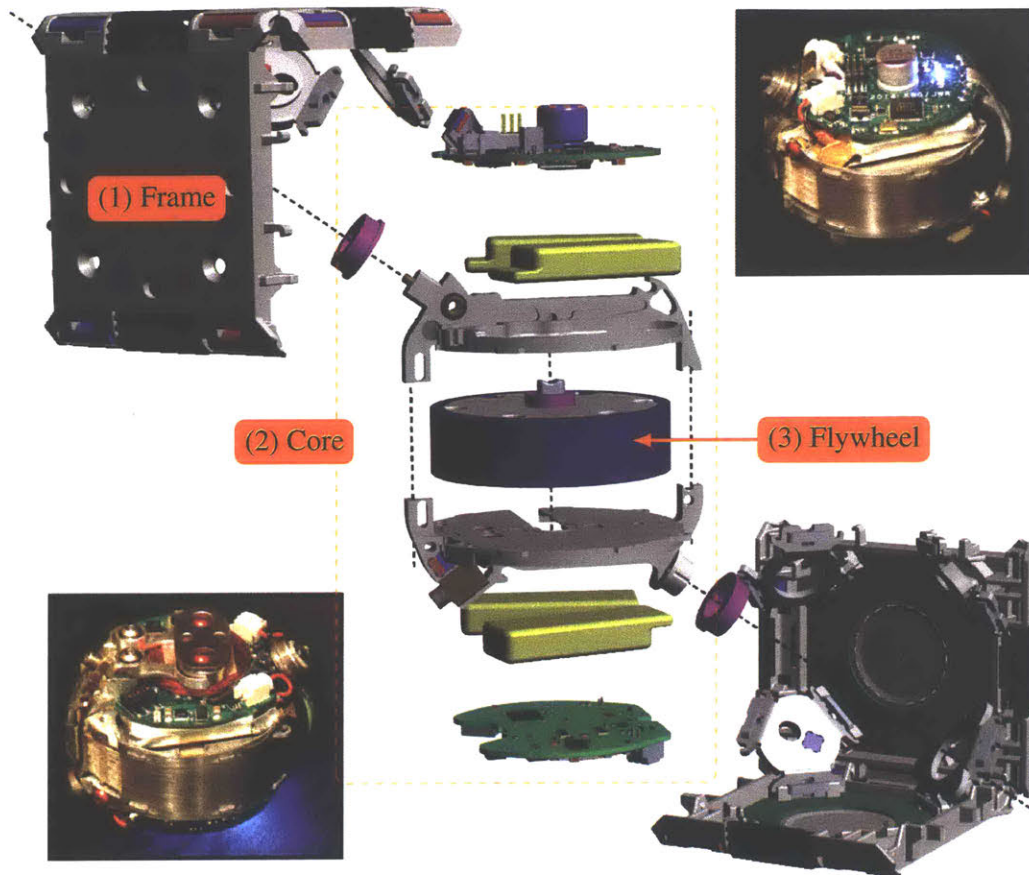
Figure 4-2: Each 3D M-Block has three primary assemblies which can be be approximated as rigid bodies for dynamics calculations including (1) The frame, (2) the core assembly, and (3) the flywheel. The frame is built out of six injection molded frame panels (*gray*) which support the core assembly (*lighter gray, split in half*) along the frame's longest diagonal axis on two ball bearings (*pink*). The molded frame holds eight magnets colored red and blue to represent their magnetic polarities for providing face to face magnetic connection with neighbors. The central assembly holds batteries (*yellow*) and circuit boards (*green*) as well as the flywheel (*purple*). The flywheel is the most important component of the inertial actuator, but for clarity the brake assembly is not shown in the exploded-view, however it can be seen in the bottom-left inset picture. This actuator uses a linear motor to actuate a band brake to generate torques. The top-right inset picture shows the core robot assembly with the main PCB side showing.

In addition, the central assembly holds the four batteries which power the module and

47

several of the printed circuit board assemblies (PCBa) which control it. The two insets in Figure 4-2 show photos of the finalized core assembly with an older version of the braking system. The braking mechanism is omitted from the exploded view for clarity and is shown in greater detail in Figure 4-6, and described in detail in Section 4.3.

At the center of the core assembly is a brushless DC motor integrated into a custom machined steel flywheel which, together with the custom designed band braking mechanism, generates the torques required for all module movements and core assembly plane changes. The entire core assembly is supported by two ball bearings on a diagonal rotational axis which extends through two opposite corners of the cubic frame. As the inertial actuator rotates about this diagonal axis, the flywheel aligns with each of one of the module's coordinate axes at 120 *degree* intervals. This design provides simplicity due to the absolute minimum of moving components, which only involve simple rotating relative motion.

Table 4.1: Comparison between the 3D M-Blocks and first generation M-Blocks on several basic characteristics. † Pre-assembled ball bearings and assembled printed circuit boards are counted as single parts.

	M-Blocks [49]	3D M-Blocks [48]
Characteristic Length	50mm	50mm
Actuation Directions	1	6
Mass	143 g	155 g
Flywheel Moment of Inertia	5.7 E-6 kgm^2	8.4 E-6 kgm^2
Total Parts †	178	239
Moving parts (Excluding edge magnets)	8	10
Unique Parts	30	71
Maximum Torque	1.6 Nm	2.6 Nm
Number of PCBa's	2	11

The mechanical design has gone through several iterations, beginning with an initial proof of concept prototype which was built in the summer of 2012 and shown in Figure 4-3 (a). This initial design was built out of laser-cut two dimensional sheets of delrin, only had a two-dimensional magnetic hinge system, and only worked several times before the braking element wore down. Following this design a more polished version, Figure 4-3 (b), was introduced as described in [49]. This version included the full 3D magnetic hinge system, but had an actuator that could only move Clockwise in a fixed plane relative to the frame. After this design successfully validated the concept of the inertial actuator

and magnetic hinges, the goal changed to attempt to create a module which could move in three mutually orthogonal planes. The first idea was to produce a module with 3 mutually orthogonal flywheels, morphologically identical to the Cubli robot presented in [21]. The challenge with this type of design is that by necessity, in order to fit three equally sized flywheels, each one needs to be pushed to the edges of three faces. This dramatically limits the potential size (and therefore inertia) of each of these flywheels. Although a three-flywheel design with enough inertia was prototyped which used flywheels made out of tungsten (with a density of 19.4 g/m^3), this design was abandoned due to the mechanical complexity after several months of work. This was followed by the final 3D System in which a single flywheel can reorient into three separate planes, as shown in Figure 4-3 (c), and described in [48]. and in Section 4.5.

(a)   (b)   (c)
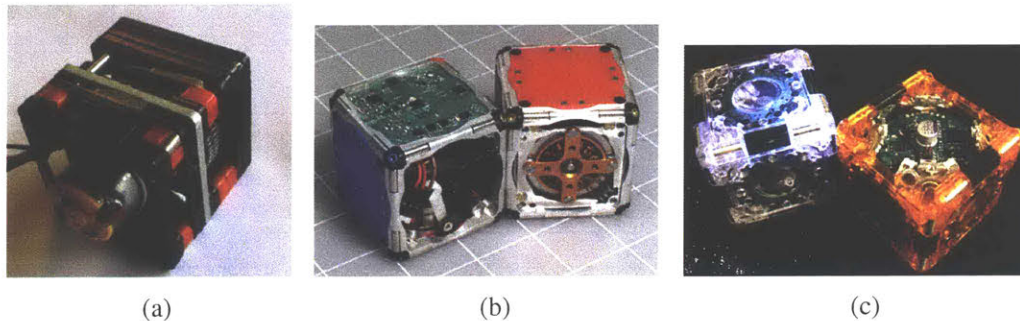
Figure 4-3: Progression of the M-Blocks module design. The first version (a) was created in 2012, and proved that the concept of inertial actuation was worth investigating further. The next version (b) was introduced in 2013, and included a full 3D magnetic hinge system, but only one axis of motion. The full 3D M-Block design (c) was introduced in 2015.

While the 3D M-Blocks have more parts and more mass than their predecessors, they are capable of producing a higher maximum torque, controlled by more robust and capable electronics, and require less expensive components. The modules have proven to be robust, undergoing hundreds of reconfiguration movements without degradation, and surviving many falls of up to one meter in height. The remainder of this section will describe the mechanical structure of the modules, the design of the inertial actuator, the operation of the plane changing mechanism, and the details of the electronics which control the modules.

49

4.2 Design of the Core Robot Assembly

The core assembly of the robot is shown in Figure 4-2 (b). This assembly is tasked with locating and protecting the inertial actuator, the electronics, and the plane changing mechanism. The primary engineering challenge for creating this structure is the conflicting goals of making the structure as stiff and impact-resistant as possible, while being able to fit many large components in a constrained volume, while also being able to be manufactured at a reasonable cost. The flywheel completely dominates the design of this assembly, as it fills up the entire center of the core assembly, and needs to be securely anchored and well protected, as it is spinning quickly relative to components in close proximity.

The first design approach was to produce two 'clamshell' like polycarbonate injection molded components as shown in Figure 4-4 (a). These components proved time-consuming to design, and required modifications after ordering to make them functional to fix oversights in how the parts interfaced with other components. However after some time, it was observed that the clamshell, and especially the coil side half, had developed a series of cracks which left it inoperable. The cracks were likely caused by a confluence of several factors; these include (1) the plastic material (polycarbonate), (2) the design of the part (cracks often formed along knit lines, and at points where the material had experienced post-machining), (3) the large impactive forces caused by the inertial actuator during reconfiguration and (4) by weak points introduced during the modifications made to the part after molding.

The entire core assembly was redesigned using metal components in light of the broken plastic frames. The final design is shown in Figure 4-5. This design consists of three components CNC milled out of 3.2 *mm* 7075 aluminum alloy which are bolted together and wrapped with a thin stainless steel band which contains the belt and provides additional structural rigidity. The main challenge encountered during this design is to make it manufacture-able and assemble-able while still fulfilling all of the functional requirements. Using high strength aluminum allows for considerable design freedom to produce components that are strong while still containing very thin sections. The design includes redundant interlocking and bolted connections between the components in an attempt to make a struc-

50
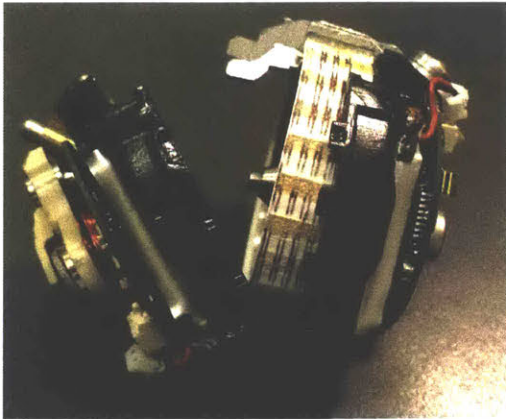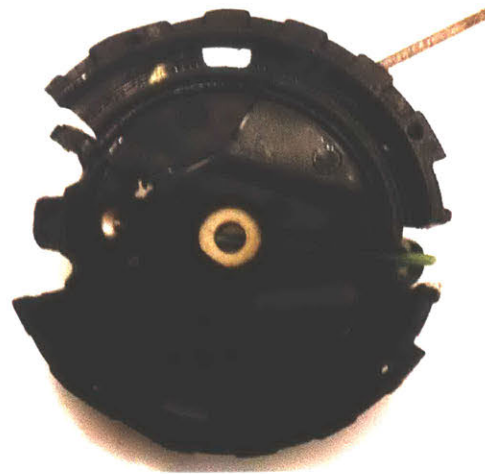
<center>(a)   (b)</center>

Figure 4-4: Initial design of the core housing (a) View of the design of the two clamshell plastic injection molded components with all of the additional parts assembled. The 'coil side' part is on the left, while the 'motor side' part is on the right. (b) View of the cracking of plastic components observed after significant use. Many factors likely contributed to this cracking, including the selection of plastic, specific design features of the parts, and the high impact forces experienced during high torque braking events. This cracking prompted a redesign of the entire core assembly to use CNC milled aluminum elements.

ture as reliable and robust as possible, in light of the many modes of vibration and impact the frame is expected to experience. This design has proved to be superior to the plastic injection molded design, as not a single structural element has broken across sixteen modules with hundreds of reconfiguration movements performed. Additionally, the motor has a higher maximum speed due to enhanced thermal dissipation from the aluminum frame. While the CNC machining operations for metal design would cost significantly more than the injection molding, the design could be modified to use either die-cast metal or impact resistant plastic in the future.

<center>51</center>

(a)   (b)
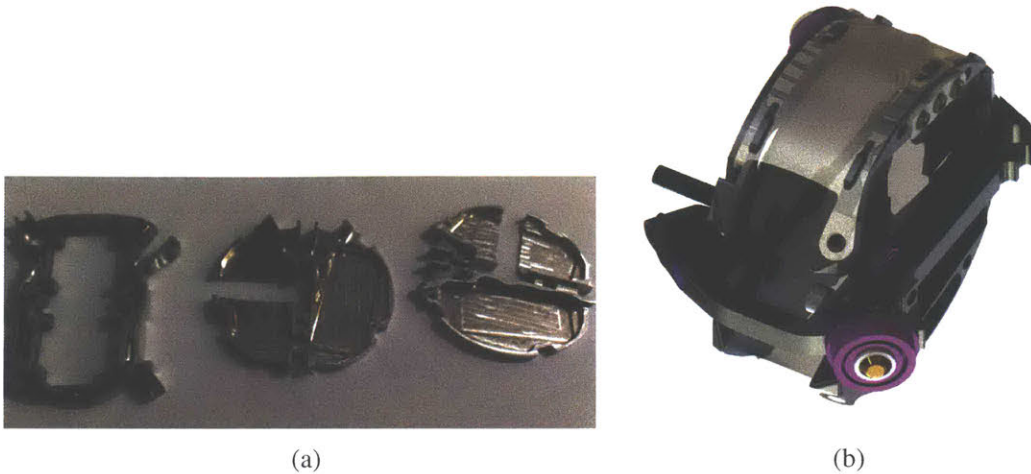
Figure 4-5: The frame was redesigned using CNC milled metal components (a) to make it more durable, and to better dissipate heat from the brushless motor. This design consists of three components CNC milled out of 3.2 *mm* 7075 aluminum alloy plate. These components together provide mounting locations for the electronics, motor, braking mechanism, and hold the two primary bearings (*pink* rings) in (b) which allows the core assembly to reorient to different planes. The primary design challenge in creating this assembly was the space constraints imposed by the need for the structure to rotate inside of the frame. This constraint effectively limits the space to be that of a sphere inside a cube which provides only 52 % of the original volume.

4.3   Pulsed Reaction Wheel Inertial Actuator

The inertial actuator is the primary generator of movement for all 3D M-Block module motions. The heart of the actuator is a 6 pole-pair brushless DC motor whose stator is integrated into a CNC turned steel flywheel. Surrounding the flywheel is a mechanical braking system which is consists of a bi-directional band brake actuated by a direct drive solenoid driven linear motor. All of the relevant components which form the actuator are illustrated in Figure 4-6. This actuator design varies significantly from the original work in [49] with a focus on replacing complex actuators with simpler ones. As an example, the actuator which moves the band brake in the 3D M-Blocks is built from a coil, two magnets, and a simple linkage. In contrast, the original M-Blocks employed a hobby-style servo motor which was large, contained many small gears, and was prone to failure.

To exert a torque on the 3D M-Block, the motor first accelerates the flywheel to a

52
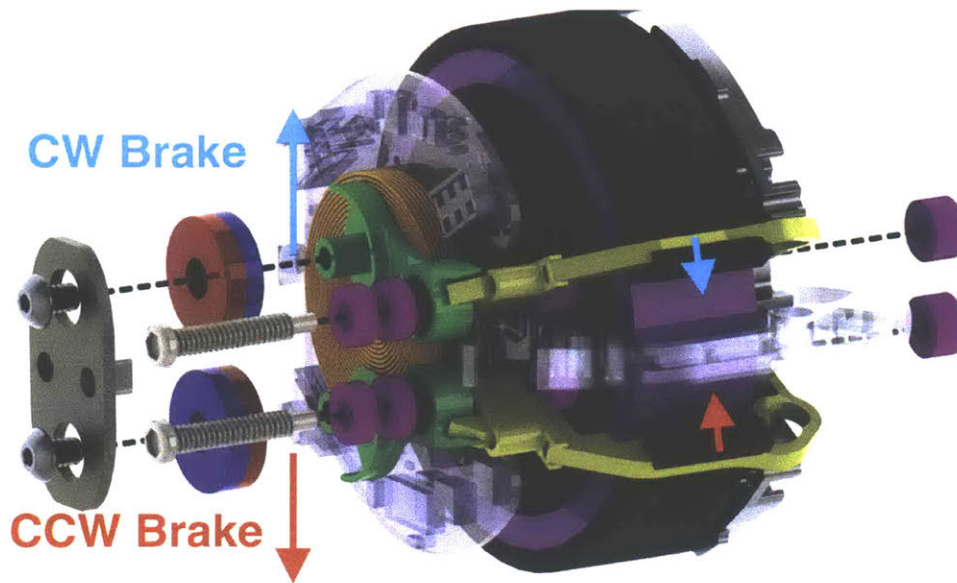
Figure 4-6: The inertial actuator operates by quickly decelerating a spinning flywheel (*purple*) with a neoprene belt (*dark gray*) that wraps around the flywheel and which is anchored in two arms (*yellow*). The belt is tightened by a linkage (*green*), which is supported by ball bearings *pink*, and which acts as a lever to amplify the force felt at the belt (*blue* and (*red*) arrows indicated relative motions for both CW and CCW braking actions). To activate the brake, the coil (*orange*) briefly generates either a positive or negative magnetic field which exerts a corresponding force on the two magnets (*red/blue*) which drives the linkage.

set speed. With the motor coasting, the module energizes the pancake-shaped coil with roughly 280 turns of #30 AWG wire to create a magnetic field. This magnetic field exerts forces on the magnetic circuit shown in Figure 4-7, with one of the magnets attracted towards the center of the coil and the other repelled. The resulting force is transferred and magnified by a ratio of roughly 1.5 to 1 by the four-bar linkage to the belt-holder arms. The two belt-holder arms are each attached in a one-way lever configuration to their respective elements in the four-bar linkage, thus allowing for bi-directional motion, despite the physical constraints of the belt-arms.

The four-bar linkage is supported wherever possible by rolling element bearings in order to maximize the force transfered from the solenoid to the end of the belt. The linkage's first two pivot arms are each supported by a pair of miniature flanged ball bearings. It was difficult to use a rolling element bearing on the the final two pivots due to the presence of the magnetic circuit, and instead they use a combination a jewel bearing with a plastic plain

<div align="center">(a)   (b)</div>
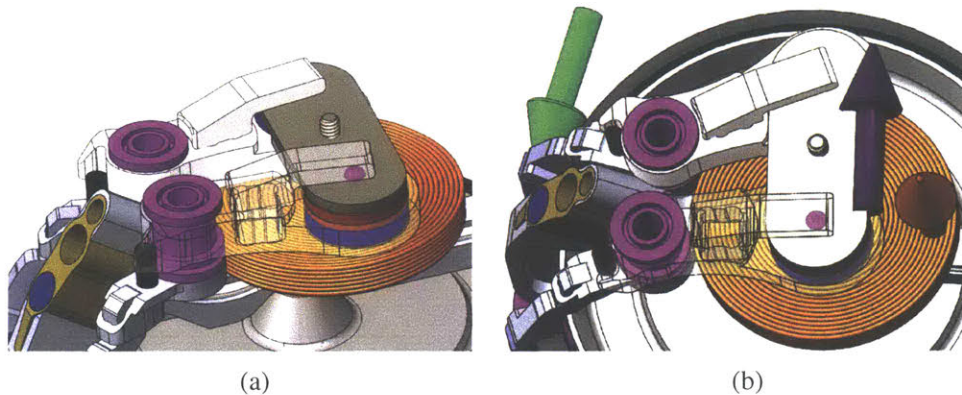
Figure 4-7: This figure illustrates the braking linkage which transfers force from the short-stroke linear motor to the braking band. Panel (a) highlights the bearings which make up the four bar linkage, including 4 flanged bearings supporting the front two arms, in addition to the combination jewel (White flexural lever arm combined with a small metal sphere) and journal bearings (provided by the arms CNC machined out of PEEK plastic. Panel (b) shows the three relevant forces during a braking event. The *orange* arrow shows the magnetic field generated by the solenoid coil. This causes a force on the far link of the four-bar linkage in the direction of the *purple* arrow. This force is transfered through the four bar linkage, and through a one-way clutch to the proper arm of the breaking band, which pulls it in the direction of the *green* arrow.)

bearing. A slight preload is applied to both bearings through a plastic flexural lever arm which pushes down on a small metal sphere, and the rotational bearing surface is provided through the CNC machined PEEK plastic arm which form the two middle links of the linkage, as shown in Figure 4-7(a). This design is careful to provide a balance between the complexity of the bearing configuration and the desire to not over- constrain the linkage.

The breaking band is composed of a segment of MXL timing belt which has all but the last two teeth cut off, which it uses to anchor each end to the *yellow* components shown in Figure 4-6. Each of these yellow parts is able to rotate independently about an axis shown as the dotted line in the Figure 4-6. They yellow arms are CNC machined out of 7075 aluminum, and are supported from the back by rigid pads built into the metal frame. This independent motion allows either of the ends of the belt to either move inward, or to act as an anchor for the band brake.

Once the flywheel is spinning, the 3D M-Blocks use a direct drive electromagnetic coil actuator as shown in Figure 4-6 to activate the brake. This approach was chosen for its

fast linear response (10 ms), adequate force (3 N), bi-directionality, low cost, robustness, and size. The current flowing through the coil is always polarized such that the end of the belt which is pulled causes the belt to constrict in the same direction that the motor is spinning. As the belt comes into contact with the flywheel, the friction between the two surfaces causes the belt to self-tighten and completely arrest the flywheel in a matter of milliseconds.

This system represents a complete redesign from the previous iteration. The redesign was necessary in order to fit the inertial actuator within the spherical constraint imposed by the re-orienting feature of the overall design. As part of the redesign, the flywheel has been made larger, thicker, and, as a result, has a higher moment of inertia which allows for larger peak torques to be applied to the module. The flexible neoprene belt used for braking is now 25% wider and 30% longer, which increases the surface area of braking contact, resulting in increased stopping power with less belt wear.

4.4   Frame and Magnetic Bonding System

The 50 mm cubic frame is built from six identical injection-molded panels which snap together. Each panel contains two functional edges which contain two diametrically magnetized cylindrical magnets. Furthermore, each panel holds eight smaller alignment magnets in the faces. The details of this magnetic interface configuration are described in [49]. This magnetic interface allows neighboring modules to pivot about the cylindrical magnets in their common edges, and to form face to face bonds.

In the 3D M-Blocks, there are 15 mm wide sections of teeth along each module's edges (shown in black in Figure 4-2). These teeth prevent slippage as two pivoting modules rotate relative to one another. Because the shape of the teeth does not protrude past the extents of the frame, it does not hinder the ability of modules to pivot next to adjacent stationary modules. Finally, each frame panel holds a face PCB which is used to interface with the surrounding environment.

Each of the eight corners of the frame contains an aluminum corner brace. These braces are water-jet cut from 1.25 *mm* 5052 aluminum sheet metal and die-formed in custom 3D

55   .

(a) Magnet schematic   (b) Actual frame
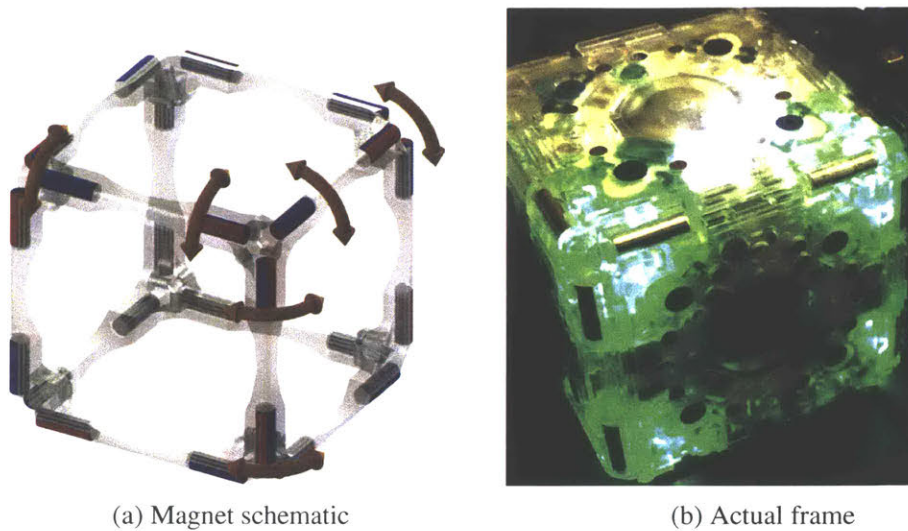
Figure 4-8: This figure shows the configuration of the magnetic hinges on each of the edges of the module. (a) 24 diametrically magnetized neodymium permanent magnets form the magnetic hinges. These magnets are held in a cage, and each magnet is free to spin along its long axis as shown with the *orange arrows* in order to align correctly with the magnets on the other module. (b) This shows a complete 3D M-Block frame with the core module inside. Each face contains a circuit board, which contains sensors, in addition to RGB LED's which can light up the corners in order to communicate with the outside world.

printed bending dies in order to rigidly connect the adjacent frame panels to each other. In addition to adding strength to the frame, two of these corner braces provide rigid mounting points for ball bearings which connect the central assembly to the frame. Three additional corner braces contain specialized mating points and magnets which are a part of the plane changing mechanism detailed in Section 4.5.

As previously described in Section 3.2 the magnet bonding system needs to provide enough force for robust face-to-face connections as well as strong edge-to-edge bonds. To provide this high strength in a small volume, N-52 grade rare-earth neodymium magnets were used. The pull strength of various conditions (as measured with a custom-built testing fixture) are shown in Figure 4-9. The pull strength of about 23N is enough to support a chain of 16 modules hanging vertically. Additionally, the torque required to separate two modules (in two different configurations) is shown in Figure 4-9(c). The high torque exhibited for the module bonded with two neighboring faces is near the limit of what the inertial actuator can overcome, therefore these moves are difficult to perform in practice.
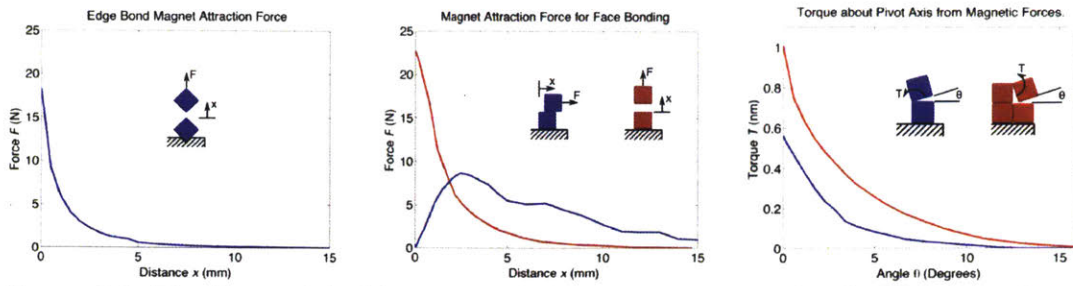
Figure 4-9: The force of the hinge strength drops very quickly after holding a maximum force of around 18 newtons (a). The force between the faces in tension *red*, and in shear *blue* are important for bonding and movement considerations (b).The torque required to rotate a module as a function of an angle from 0 to 16 degrees (c). The torque required in four module configuration is large enough that the current actuator has difficulty pivoting the module.

However there are a number of relatively simple ways that this could be overcome, from recessing the magnetic hinges further into the frame, to using an inertial actuator with higher peak force.

(a) Panel detail   (b) Corner brackets
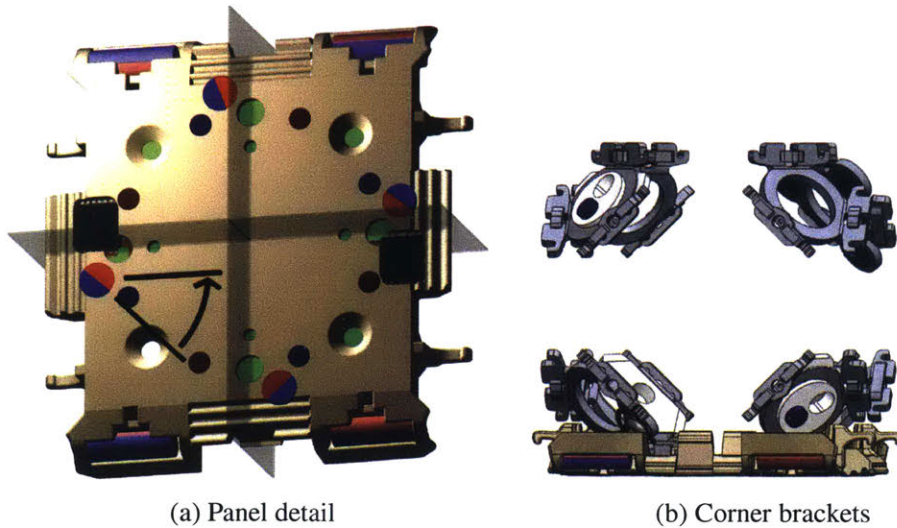
Figure 4-10: This Figure shows several different views of the 3D M-Block module's frame. (a) Shows a detail of the injection molded panel, The notable elements are the cages which hold the edge magnets, and the teeth in the middle of each edge, which are formed halfway by each of the panels. These teeth help the modules to stay aligned during reconfiguration movements. (b) Eight sheet metal brackets anchor the eight corners of the frame, and provide mechanical connection points for the core assembly.

4.5 Multi-Plane Actuation Ability

The central assembly in each 3D M-Block can be thought of as a sphere rotating inside of a cube (the frame). In order to fully constrain the two assemblies together, three points of contact are required. Two of these points are formed by ball bearings attaching the central assembly to the frame through an axis aligned between two opposing corners of the frame (along the long diagonal). This diagonal axis is offset by 0.46 radians from that of the flywheel's axis of rotation. This diagonal axis extends through two bearings placed in brackets on opposite corners of the cubic frame. As the central actuator rotates every third of a complete revolution about this diagonal axis, the flywheel aligns with a different set of the module's faces. That is, if the flywheel is initially aligned with the module's x-axis, rotating the core assembly by $2\pi/3$ radians, in one direction or another, will bring the central actuator into alignment with the module's y or z-axis. These three possible positions are shown in Figure 4-12.

To lock the central assembly into place, a third connection point is necessary. This connection is formed by a retractable pin which protrudes from the central actuator. When extended, the pin locks into with one of three matching pockets in the frame's corner braces (see Figure 4-12). This pin is connected to a 100 *mm* section of FLEXINOL brand 0.25 mm shape memory alloy (SMA) wire, which when heated retracts and pulls the pin inwards. The SMA wire is contained within a heat-resistant, insulating PEEK plastic tube. This tube insulates the wire from the metal structure of the central assembly, and it also allows the wire to bend a complete π radians in order to fit the necessary length of wire within a the constrained area of the core assembly. One end of the SMA wire is electrically connected to a constant current driver on the power control circuit board. The other end of the wire is crimped into the retractable pin, which touches the central aluminum frame, and provides an electrical ground. A strong (425 N/m) spring provides the necessary restoring force to extend the pin when the SMA is not being heated. As such, the SMA only consumes current when the pin is being held in the retracted position.

58

(a) Frame points

(b) Retract pin

(c) Apply torque

(d) Torque components

(e) Rotate

(f) Lock into place
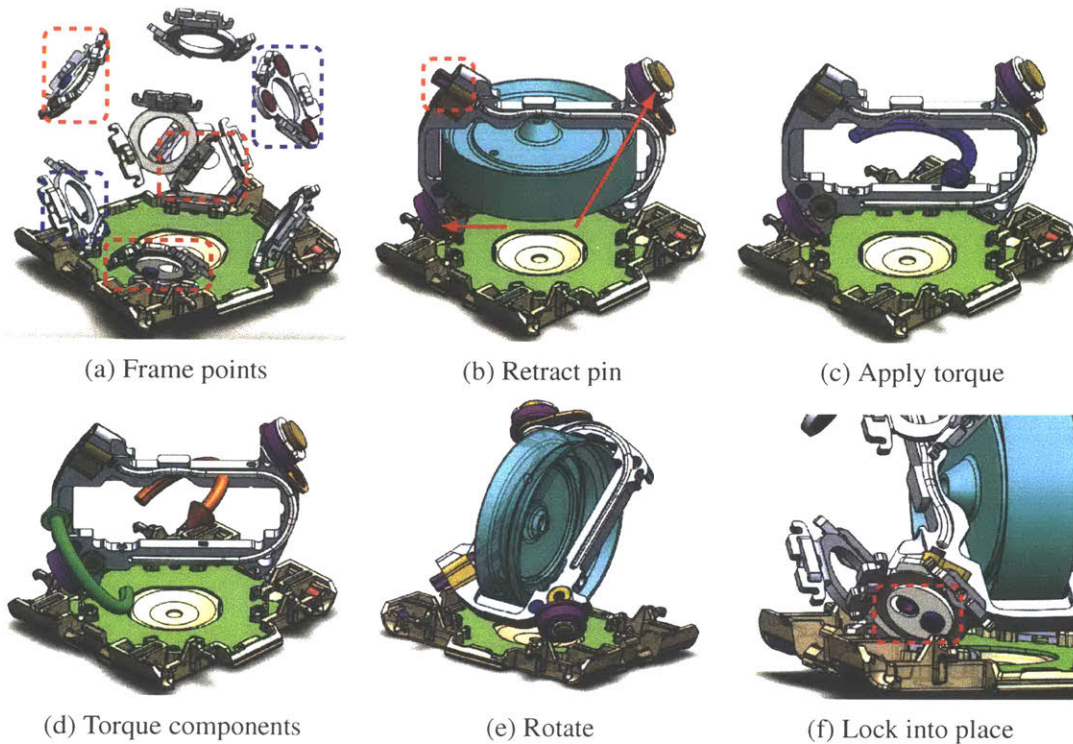
Figure 4-11: Plane changing sequence diagram, illustrating the major steps involved with transitioning between planes. There are five connections points between the frame and the core (a), with only 3 being used at a time. Two metal brackets (*blue dashed*) support ball bearings to with three potential anchor points shown in the (*red dashed*) rectangles. In the first step, shown in panel (b) the pin (*red* dashed box) is retracted by a shape memory alloy wire. Now the core assembly is able to freely rotate about the two bearings (*red arrows*). Next a torque is applied to the core, panel (c), as depicted by the *blue* curved arrow. This torque can be decomposed into the *orange* and *green* arrows. With the torque represented by the *green* arrow inducing motion about the primary axis. In panel (e) the core has rotated to a new plane, and is caught by one of the neodymium magnets embedded in each of the three potential connection points. Finally, in panel (f), the pin extends and securely locks the core assembly into the new plane.

In order to switch planes, the 3D M-Block first spins-up the motor. Once the flywheel has reached a constant speed, the pin is retracted, which allows the central assembly to spin freely on its diagonal rotation axis. A torque is then generated by electronically braking the motor. The component of this torque aligned with the diagonal axis causes the central assembly to rotate and align into a new plane. Magnets, one embedded in the central assembly, and one next to each of the pin alignment pockets in the frame, provide magnetic detents to assist with fine alignment between the central assembly and the frame. Once

the pin is aligned with one of the mating pockets, it is then extended to lock the central assembly into place in the new configuration.

(a) X-axis   (b) Y-axis   (c) Z-axis
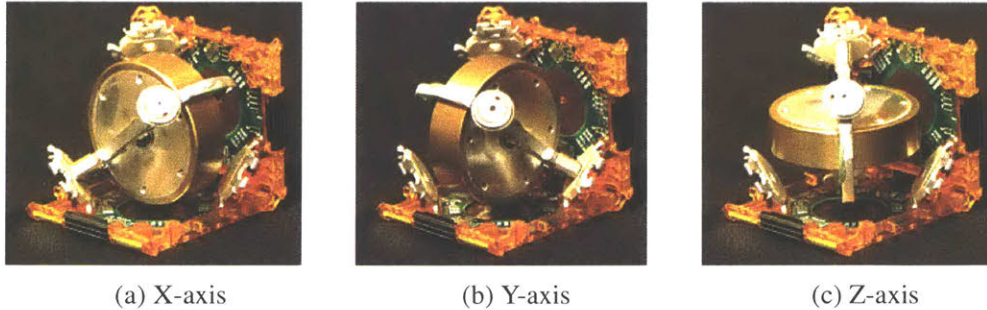
Figure 4-12: The 3D M-Block changes the alignment of its flywheel by rotating the central assembly along a diagonal axis between two opposite corners of the frame (pointing out of the page). For every $2\pi/3$ radians of rotation along this axis, the flywheel comes into alignment with a new axis of the frame.

During experiments with the 3D M-Blocks, the central actuator sometimes stopped rotating about the diagonal axis at points which left the pin misaligned with the mating pockets in the corners of the frame. To counteract this, additional repulsive magnets near one of the bearings complement the attractive force already provided by the magnets near the pin mating pockets. While this change greatly reduced the frequency with which the central actuator ends up misaligned with the frame, it has also made it difficult for a module to change the plane of its central assembly if the module is not magnetically attached to a larger lattice, since these magnets essentially provide a higher spring potential energy well which has to be overcome in order to reach a new plane. Without additional mass to help immobilize the module, attempting to change the plane of the central actuator when it is not connected to a lattice results in the entire module pivoting about one of its edges, or just moving randomly.

4.6 Electronics System Design

The electronics system which control each 3D M-Block is divided across eight different primary PCBs. The high level functionality is provided by a PCB based on an ESP8266 WiFi module running code written in the Arduino language. A high level overview of the

electrical system is shown in Figure 4-13. The primary reason for the complexity of this design is due to a change of design requirements during the multi-year long development of the 3D M-Block modules. Due to a complicated situation with the memory on the original board used to provide the high-level controls for the modules, and a desire to simplify the programming of the modules, the additional ESP8266 control board was designed and fabricated as a last minute addition. This created unnecessary complexity since the high level board does not have direct control of the motor and actuator control circuitry. The rest of this section discusses in detail the multiple circuit boards in each module.
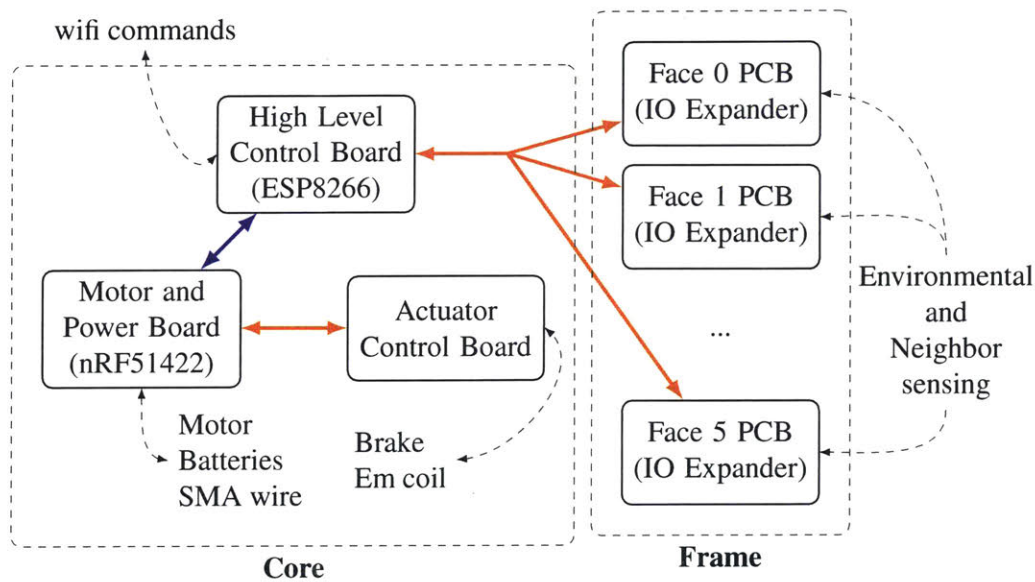
Figure 4-13: This Figure diagrams the somewhat convoluted electronics system in each 3D M-Blocks. There are a total of 9 separate primary circuit boards, shown as rectangular boxes, with 6 being almost identical boards located on each of the six faces of the module, and the other three managing and controlling all the power, communications and actuators. There two separate I2C communication networks (*orange arrows*), and one serial connection (*blue arrows*). One of the difficulties with this setup is that some of the boards were designed and built before the design was finalized, leaving an unnecessarily complex system which has led to complicated electronic and programming problems.

4.6.1 Main Controller Board

The main controller board fits on-top of one of the two power boards, and is shown in Figure 4-14 (b) and was added after the design of the other two boards in order to add new
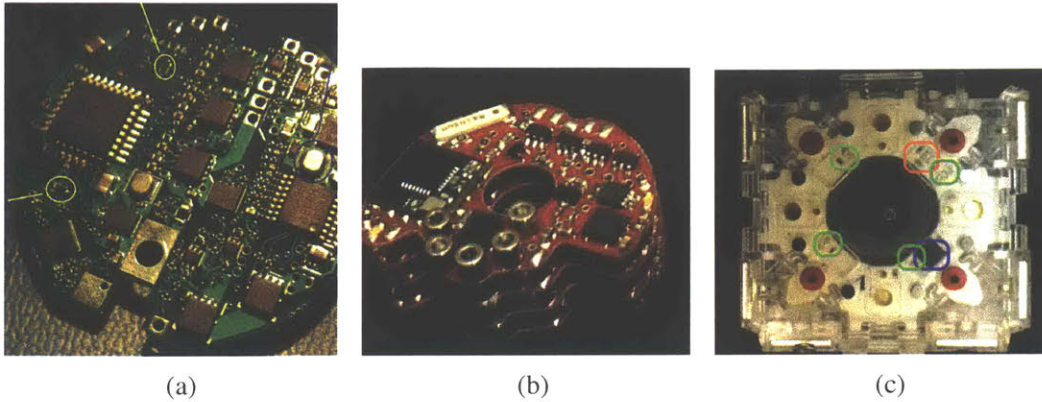
Figure 4-14: (a) Actual circuit board kyle built (b) controller circuit board (c) face circuit boards

functionality without a complete re-design of the power and actuator management PCBs. This board is centered around a pre-assembled ESP8266 module built by the company Expressif. This small module (10x10mm) contains the ESP8266, which is an arduino-programmable microcontroller in addition to dedicated WiFi radio hardware. The modules are able to form their own WiFi mesh network in order to communicate with each other in addition to a base station module for centralized control. This microcontroller also controls an I2C bus which manages a MPU-6050 inertial measurement sensor in addition to a the circuit boards on each of the six faces. There were several electrical difficulties involved with interacting with the main actuator boards, especially considering one of the wires which connects the frame to the core serves dual use as both a charging cable and as the main power supply to the face boards. The details of this switching circuitry, created after significant trial and error, can be found in the schematic labeled *M-Blocks Main Board* in Appendix A.

4.6.2 External Sensing and Interaction Boards

The face PCBs, Shown in Figure 4-14 (c), are electrically connected to the central assembly by custom slip rings formed by the bearings that support the central assembly. One bearing is in direct electrical contact with the central assembly and provides a ground connection, while the other is isolated and carries one of the bus lines to the face PCBs. The two addi-

tional sliprings are implemented using a electrical spring pin contact which pushes against a machined brass pad at the center of each of the two bearings. Experiments have shown that the bearings present several ohms of resistance. However, the face PCBs do not require high currents, so this is not problematic. When power is flowing into the central assembly during the charging process, the voltage drop across the bearings can be compensated for by an increase of the external charging voltage.

The face PCB's are designed to communicate with the main controller board through an I2C bus. This bus connects with six IOexpanders with unique hard-wired addresses on each of the six nearly identical face boards in order to sense the environment and neighboring modules, in addition to activating LEDs for communicating the internal state of the module to an outsider. This I2C bus also supports an additional MPU6050 inertial measurement unit which is mounted to face number 0. By comparing the vector of this accelerometer with that of the accelerometer on the main controller board, the relative angle between the core assembly and the frame can be uniquely determined.

4.6.3   Motor and Power Management Boards

The motor and power management boards consist of two PCB's connected to each other by a high voltage (16 V) power connection and an I2C bus, and is shown in Figure 4-14 (a). The main PCB is based on a Nordic nRF51422 (nRF) microprocessor with an on-chip 2.4 GHz radio. The power and actuator management PCB's manage the battery and charging system and all of the actuators, including the brushless motor, SMA driver, and the driving of the solenoid coil used for mechanical braking. The central brushless motor control is managed by a dedicated Allegro MicroSystems A4960 which frees the main processor for higher-level tasks. While the A4960 handles the low-level motor control, closed-loop speed regulation requires supervision from a the nRF microcontroller. The flywheel brushless motor is controlled in a sensor-less configuration, which limits its performance at low speeds. The A4960 can apply an electronic braking torque to the motor in order to decelerate it more slowly than the mechanical brake. This board also contains the circuitry to manage the retractable SMA based pin used for plane changing. This circuit

is based on a high-current LED driver and a low-side current sense amplifier. It is capable of driving a maximum of 1.5 A through the SMA wire, but due to the relatively slow thermal response of the SMA, the current is modulated on and off to achieve sufficient force without overheating the SMA wire. When retracting the pin, an average of 1.2 A for 2 s is required, but once retracted, the SMA draws an average of only 700 mA.

This PCB also includes charging and balancing circuitry for the four 125 mAh lithium-polymer batteries which power each 3D M-Block. The batteries are connected in series in order to supply sufficient voltage to drive the motor at speeds over 15,000 RPM. Charging is enabled by connecting the 3D M-Block to a 5 V, 500 mA source (e.g. a USB port). An on-board, current-limited boost converter controls the voltage and current delivered to the batteries. If the nRF detects that one battery's voltage is exceeding that of the others, it switches in an additional resistive load across that battery thereby reducing its charge rate and keeping all batteries balanced. A battery protection IC independently monitors each battery's voltage and current drain and disconnects all batteries if it detects a fault condition. The main PCB also includes additional reverse-voltage, over-current, over-temperature, and electrostatic discharge protection devices in recognition of the fact that the 3D M-Blocks must remain robust when being deployed outside of the laboratory environment.

To complement the main PCB, there is a daughter PCB attached to the opposite side of the central actuator. The two PCBs communicate over an I2C bus with the nRF acting as the bus master. In addition to providing the connection point for two of the four batteries, the daughter PCB holds the circuitry which drives current through the mechanical braking coil. This braking circuitry is controlled by an STMicroelectronics STM32F051 microprocessor which is a slave on the two-wire bus. The braking circuitry is based on an op-amp which linearizes a current-controlling PMOS device in order to provide continuous current control from 0 to 6 A.

Chapter 5

Experimental Results

This chapter presents the results of both system-level experiments and hardware characterization for the 3D M-Block system. Sets of lattice experiments were performed on one representative module, and the success rate of each movement in is shown in Table 5.1. Additionally, the torque profile of the inertial actuator under several different input parameters was experimentally measured using a reaction torque sensor. Finally, several less formal experiments involving 3D M-Blocks moving independently and as assemblies are presented. This chapter is based on the experiments conducted in [48], and does not reflect changes to the 3D M-Blocks hardware since that work was published.

5.1   Hardware Characterization

This section details experiments involving characterization of the hardware subsystems on the modules. The performance of the inertial actuator (Section 4.3) as well as the plane changing mechanism (Section 4.5) are discussed. The inertial actuator can generate torque through electronic braking, as well as through the mechanical band brake described in 4.3, and both are characterized and discussed.

5.1.1 Characterizing the Inertial Actuator

In order to reconfigure the 3D M-Block about a lattice structure, a torque is required which is powerful enough to overcome the substantial magnetic bonds attaching the module to its neighbors, but not so powerful that the module disconnects from the structure completely. The inertial actuator can generate torque through two methods; accelerating or decelerating the flywheel electronically, or by application of the mechanical brake to the rotating flywheel. As shown in Figure 5-2, the acceleration and the electronic braking of the flywheel generate for a period up to 1 s maximum torques on the order of 0.03 Nm, and 0.04 Nm, respectively. While these torques are not sufficient to perform any lattice reconfiguration movements, they allow the module to locomote independently, and to change planes. The application of the mechanical brake, in contrast, generates torques over a much shorter duration (10–30 ms) but which approach a maximum of 2.6 Nm. This magnitude of torque allows the modules to perform all but the most difficult lattice moves. For example, an upward stair-step while connected by four faces (bottom, front, left, and right) is not currently possible.
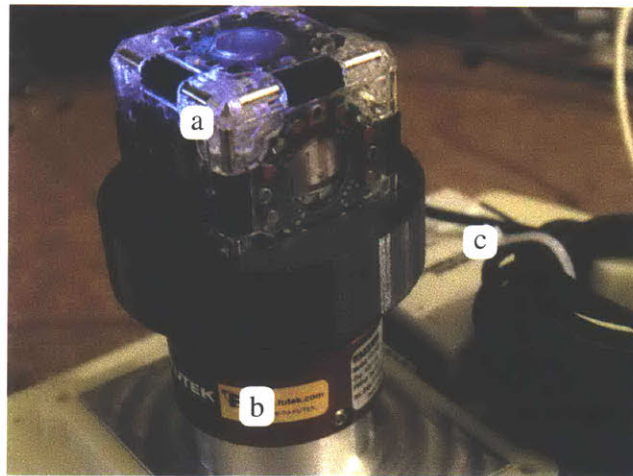
Figure 5-1: This figure illustrates the experimental setup used to characterize the inertial actuator. The module (a) is connected to a FUTEK TFF500 reaction torque sensor (b), and is digitized by an NI DAQ (c) at a sample rate of 10 kHz.

The mechanical brake generates torque through a self-tightening band brake as described in Section 4.3. The torques generated by the mechanical brake display inherent
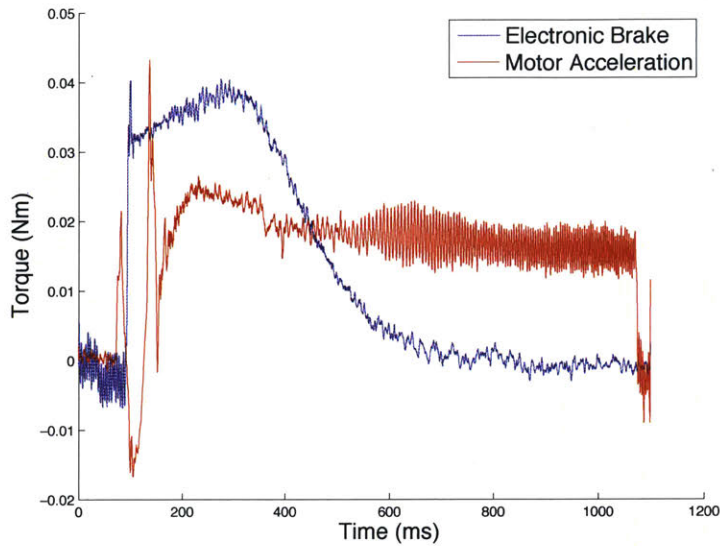
Figure 5-2: This graph shows the torques generated by the inertial actuator through acceleration and electronic braking, without any use of the mechanical brake. Braking is accomplished by essentially shorting the motor wires together using the built in functionality of the motor control IC. These torques are sufficient to move a single module across the ground in an unstructured environment. Additionally, these torques are sufficient to cause the central assembly to change planes when the locking pin is retracted.

variability due to manufacturing tolerances of the components amplified by the non-linear nature of many of their interactions. The module does not have closed loop control of the output torque from the actuator, and is run in an open loop configuration. There are three separate selectable parameters which govern the braking event; the flywheel rotational speed (up to 16000 RPM); the current supplied to the brake (up to 6 A); and brake actuation time (up to 250 ms). A characterization of the torque generated with the mechanical brake under several different control inputs combinations using a load-cell based Futek TFF500 torque sensor as shown in Figure 5-1 sampling at 10 kHz is shown in Figure 5-3. Although a more detailed exploration of the mapping between all of the inputs and the resulting torque would be valuable, sufficient input parameters for most lattice movements have been determined through trial and error. Since the values for lattice reconfigurations were experimentally determined, the repeatability of an output given the same input is important for consistent system performance. A qualitative sense of the repeatability of the actuator can be seen in Figure 5-3. While Figure 5-3 only shows data from a single cube,

there is additional variability between the actuators of different modules. This variability could be mitigated through more consistent manufacturing and potentially a simpler design of the braking assembly which decelerates the flywheel.
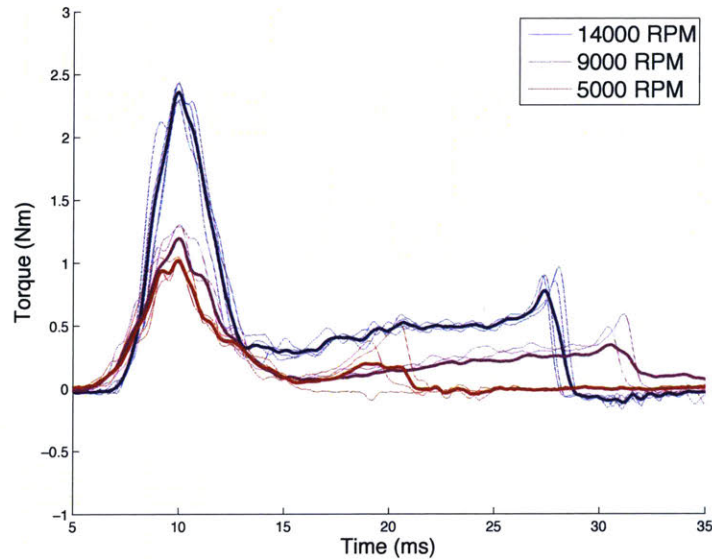
Figure 5-3: This graph shows the torque generated by the inertial actuator for different input parameters measured at a rate of 10 kHz. The bold line represent the mean values of the torque. The 14000 RPM experiment actuated the brake with 4000 mA current for 250 ms, while the 9000 RPM, and 5000 RPM experiments actuated the brake for 2000 mA for 250 ms.

5.1.2 Plane Changing

The plane changing process is under-actuated, (see Section 4.5), and it behaves in a somewhat stochastic way. In order to change planes, a torque is applied using the electronic brake while the locking pin is retracted. This torque causes the core assembly to begin to rotate about its axis of rotation, until it finally stabilizes. After the central core has started to rotate, the two IMU's are sampled, and the main processor calculates whether the intended orientation is as desired. In the case that it does not achieve the correct orientation, the module continues trying to change planes until the correct orientation is achieved. Ten experiments were performed in which the commanded plane was cycled through the three possible orientations. The module was able to correctly align its orientation in all

ten attempts, with an average time to do so of 21.7 s, with a standard deviation of 17 s. Currently the ability to change planes works optimally while the module is attached to a lattice structure, although it is still possible while the module is independent.

5.2 System Level Characterization

This section presents experiments testing lattice reconfigurations as well as initial tests of more challenging maneuvers. The lattice experiments are reproduced from [48] in 2015, and may not reflect more recent changes to the 3D M-Blocks hardware.

5.2.1 Lattice Reconfiguration Experiments

The primary goal of the 3D M-Blocks is to provide robust lattice reconfiguration. Table 5.1 demonstrates the results of a range of different attempted motions. The values of the feed-forward braking parameters for each movement were found through trial and error. A motion is considered a success if after three attempts it can successfully move to its desired lattice position without exhausting its battery or disconnecting from the regular lattice structure. There are many factors which are important to movements that seem to vary randomly, including many which are difficult to measure, including the exact force in each bond, as well as the precise torque profile from the specific actuator involved. These vary on a module-by-module basis and with the exact system configuration, and future attempts to allow self-calibration for each module might help to improve the reliability of these moves.

A series of nine representative lattice reconfiguration experiments with a single module were performed as shown in Table 5.1. Each reconfiguration movement was tested at least twenty times, and the overall success rate for all of the motions combined is over 88%. The success rate has increased for every movement as compared to the corresponding experiments in [49], except for the horizontal traverse, and the horizontal concave motions; see Table 5.1. The success rates of these motions was lower, which can be attributed to the higher module weight, and interference with the edge teeth while performing rotations of π radians. Additionally, the modules are now able to perform the stair step motion which

requires more torque than the previous 3D M-Blocks were able to provide. However there is anecdotally significant variability in the ability to perform this move between different modules, as it requires close to the maximum torque which each module can provide. Since the pivoting motion exerts significant forces and torques on the entire lattice structure, some of these motions will not perform as tested under differing lattice configurations. For example, if the lattice contains only a few modules, it may be too weak to maintain its structural integrity during some transitions, or it may not be massive enough to serve as an immobile substrate on which individual modules move. Generic 3D lattice reconfiguration will be possible in a system containing many 3D M-Blocks, as long as the motion planner is capable of recovering from occasional movement failures, and optimizing for a sequence of moves which have the highest reliability.

Table 5.1: Experimental results for controlled tests of various motion primitives are shown. These tests were performed on the hardware presented in [48]. Some of the move reliability performance has decreased on the more difficult moves such as the stair step, the Vertical Traverse, and the Vertical Convex, likely due to the additional weight that the modules have picked up due to extensive circuit board changes. (a) Traverse, (b) Horizontal Traverse, (c) Vertical Traverse, (d) Horizontal Convex, (e) Vertical Convex, (f) Horizontal Concave, (g) Vertical Concave, (h) Corner Climb, (i) Stair Step.

	(a)	(b)	(c)	(d)	(e)	(f)	(g)	(h)	(i)
Attempts	41	20	20	20	20	20	20	20	20
Success	100%	70%	80%	95%	100%	55%	90%	100%	95%

5.2.2 Additional Experiments

In addition to the individual module lattice reconfiguration moves presented in Table 5.1, several additional movement capabilities have been tested in a less rigorous manner. The 3D M-Blocks are able to move independently using several motion primitives. While moving independently of a lattice (e.g. on the ground), 3D M-Block modules are able to move forward or backwards along the actuator plane in steps ranging from a single controlled roll about an edge (50 mm), to a more stochastic single movement of up to 1.5 m at full actuator

power. Additionally, when the inertial actuator is oriented parallel to the ground plane and the motor is quickly accelerated for 1 s, the modules perform a random walk by rolling about their corners, and travel a distance of approximately 0.5 m along a random heading while coming to rest in a random orientation. Using these movements, the 3D M-Blocks should be able to disperse, thoroughly explore an environment, and then re-combine into a single structure.

(a)   (b)
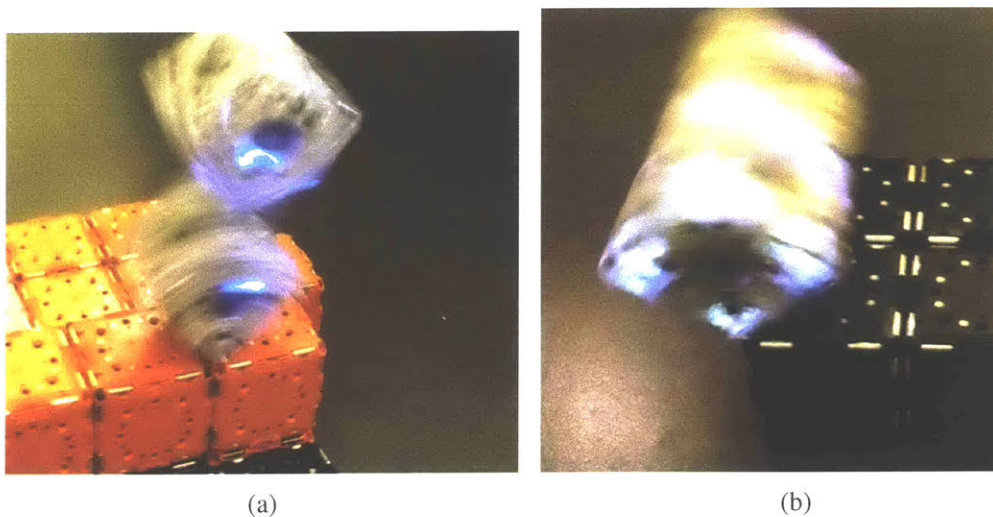
Figure 5-4: Additional lattice experiments (a) double roll (b) two 3D M-Block modules performing a corner climb move sharing the same pivot axis. The double roll experiment was attempted many times, and was rarely successful. The reason for this low success rate is that there is not currently a mechanism to synchronize the time of the braking events between the two modules.

Multiple 3D M-Blocks are able to perform lattice reconfiguration movements in parallel as a meta-module. Several proof of concept experiments with two modules executing a coordinated traverse have been performed, as seen in Figure 5-4. It was even possible to perform a double roll, with the modules acting in a similar manner to a double inverted pendulum, Figure 5-4(a). However this was very rarely achieved over many attempts. In order to reliably perform coordinated movements, some method of consistently synchronizing the timing between modules will need to be developed.

Chapter 6

Discussion and Future Work

This thesis presents work on a new modular self-reconfigurable robotic system, the 3D M-Blocks, which uses a custom designed inertial actuator to reconfigure modules on a cubic lattice through pivoting motions. Over the course of working on this system, many difficulties involved with creating MSRR systems have become apparent. There are many fundamental issues with the design of the current system, and with systems based on dynamic pivoting motions in general. These issues and limitations in addition to some specific lessons learned and future work ideas are addressed in this chapter.

6.1 Challenges and Limitations

Although the 3D M-Blocks have contributed several innovations to the field of MSRR, the system must overcome many serious challenges before it will ever be practical. There are many problems with the current hardware, some of them stemming from design decisions made early in the development process. These are covered in more detail in the next section, but they include electrical system complexity and the wide variance in the performance of the inertial actuator and magnetic system from module to module. Additionally there are important practical challenges that have been omitted from this proof of concept system. These include the lack of any mechanism to rigidly connect modules together beyond permanent magnets, and the lack of any electrical power sharing system. Adding these systems might prove to be more difficult than initially imagined. Besides the

73

difficulty of physically fitting these additional systems in with all of the existing hardware, in light of the dynamic constraints discussed in Section 3.2, as the modules become heavier all reconfiguration motions become more difficult.

The development and implementation of algorithms to guide reconfiguration also present many challenges. Although algorithms have been proposed for reconfiguring 3D M-Block modules according to Pivoting Cube Model [61], these algorithms have not yet been implemented on the actual 3D M-Block hardware. Additionally these algorithms do not factor in any of the practical considerations involving dynamics of the pivoting motions, or the stability of the larger lattice structure. The inter-module bonds in a structure must be able to withstand the impulsive forces experienced during reconfiguration, which may often exceed the static bonding forces. Consequently, a planner which accounts for the impulses experienced during reconfiguration may prove necessary. The most feasible path to developing an algorithm that can work on the actual hardware would involve determining which moves in which circumstances are the most likely to succeed, and then prioritizing those moves when generating a motion plan. However it is unknown if the constraints provided by actual physical hardware systems will be too limiting in order to generate useful general reconfiguration algorithmic.

The entire idea of modules moving through pivoting also potentially has certain serious challenges. While the use of magnetic hinges dramatically simplifies the mechanical design of the modules, it could prove dangerous in practical use as modules could fly off of the structure and cause damage. Additionally the current system and movement framework has no method of actually manipulating the world, as many of the other MSRR systems, especially those that are based on kinematic chains, are able to. While one could imagine a heterogeneous system (i.e. one with many different types of modules) which could combine pivoting with more traditional rotating joints, developing algorithms for such a system would be very challenging. Despite all of these challenges, hopefully this work will be able to provide the foundation for a lattice-based modular robotic system which is robust, simple to use, and capable enough to work in the real world.

6.2 Lessons Learned

While working, and sometimes struggling, on this project for the last 5 years, I have learned many important lessons. It is my strong belief that the more times one is forced to face the consequences of one's mistakes, the more deeply one learns the underlying lesson. This project has given me many of these types of lessons. Designing and actually manufacturing just a single prototype of a complex electro-mechanical system is difficult enough on its own. However I have learned that building and creating sixteen copies of the same device is a significantly more challenging problem to solve. Everything that can possibly go wrong with the initial design is painfully revealed repeatedly as each new device is built. Since there are so many different components in different stages of being built and manufactured, it is difficult to redesign anything without redesigning everything. I now have more respect for any industry that actually mass produces complex systems of any kind.

The following list includes some of the lessons that I have learned while working on this project:

1. Tolerances are important. There was an attempt to be too greedy in the design by attempting to maximize the size of the core of the module relative to the frame. Due to manufacturing and assembly tolerances, the core often collided with parts of the frame, which required a tedious manual filing process to fix. A difference of around a quarter of a millimeter could have solved a large set of problems involving plane changing.

2. Electrical connectors are challenging, and should not be a design afterthought. Many of the reliability issues with this system involve the points where electrical wires connect from one element to another, such as battery connectors which come loose and don't solder correctly and slip-rings which cause random disconnects and resetting and shorts in the electrical systems.

3. Kludging together systems will often take more time in the long run that going back and redoing everything the correct way. This is especially true with electronic circuits. A quick look at Figure 4-13 illustrates an example of this problem in action.

There is actually one point where there is a stack of three separate PCB's in one large sandwich because some parts of the design kept changing.

4. Reliability should be the number one design goal when building systems with many repeated elements. As a thought experiment, there are approximated 250 unique parts in each 3D M-Block, giving a total of 4000 total parts for the system of 16 modules. If the chance of a specific component breaking is even 1 in 1000 in an hour, one of the modules will break every 15 minutes!

6.3 Future Work

The long term goal remains to create a system which can actually built useful structures in the real world. However the path getting to this point is unclear. In the more immediate term, there are improvements which can be made to the current modules along two lines, developing simpler electronics, and developing a more reliable and capable inertial actuator.
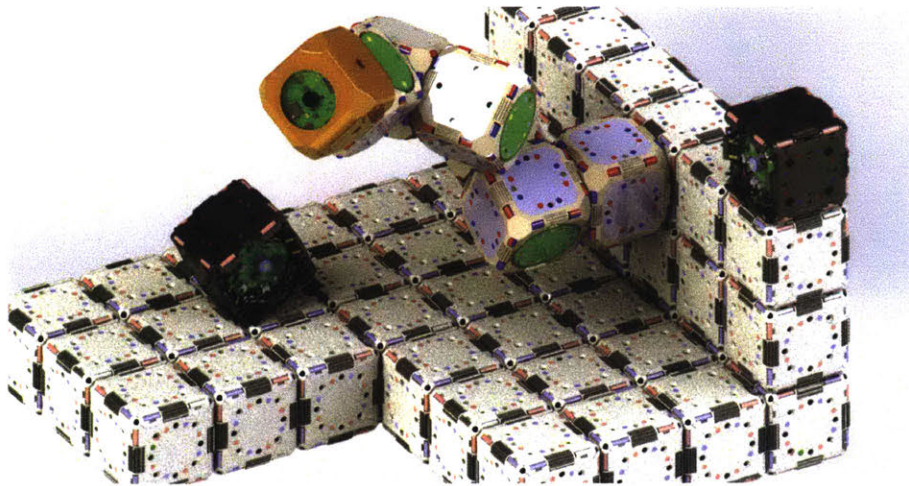
Figure 6-1: The future vision of this work is to create and build modular systems which include heterogeneous collections of modules, with different modules accomplishing specialized tasks. In this example modules which function as servos combine with 3D M-Blocks to explore an unknown environment. The goal is to create a robust and simple set of specifications in order to allow different groups of modular robots to work together in an open-source manner. Creating such a standard has proven challenging in the MSRR field to date, but is the primary motivation for future work.

While the inertial actuator described in Section 4.3 works to some degree, it is not very reliable, takes up significant physical volume, and has too many complicated (and expensive CNC machined) moving parts and linkages. The reason why this actuator was designed this way is that there was a perceived need for a large force to pull the end of the band which brakes the flywheel. Because of the design goal for this actuator to be able to generate large forces, the actual element which generates the force, the electromagnetic coil, was placed relatively far from where the force ultimately is applied to the band. The mechanism required to bridge this distance involves the use of no less than 6 sealed ball bearings, 4 sliding bearings, 8 small custom CNC machined aluminum components, and lots of tedious manual assembly. However because the actual braking events only last on the order of 10 to 20 milli-seconds, it should be possible to dramatically shrink the size of the braking coil, and place it directly adjacent to the ends of the belt. In addition to making the design far simpler, this change could also dramatically increase the consistency of the mechanical brake, as there would be a more direct chain of force transmission elements involved in actuating the brake.

(a)   (b)
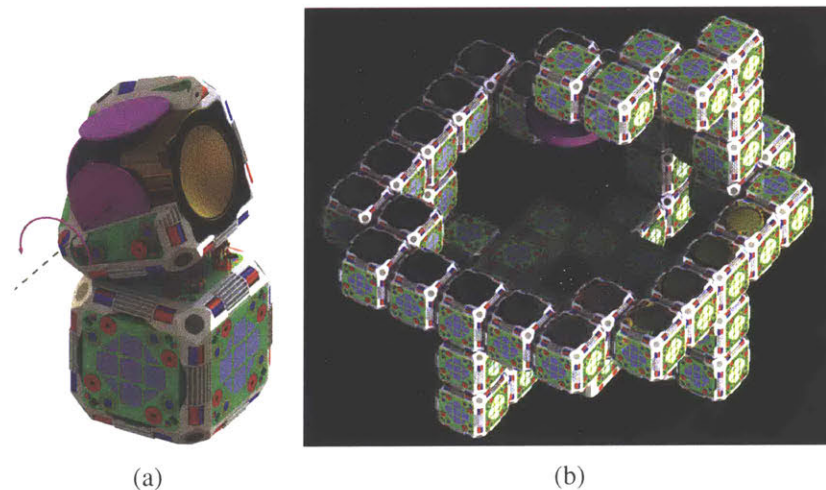
Figure 6-2: One potential research direction would be to attempt to apply the principles learned in developing the 3D M-Blocks to a system which is more suitable for space applications. These renderings show what an M-Block inspired reconfigurable space telescope might look like.

One additional promising area of research is in creating reconfigurable structures for space. Much of the existing modular robotics research has focused on space at least as a

long term motivating goal. Several systems, most notably the work developing a reaction wheel powered modular satellite [56], have attempted to address some of the many engineering constraints inherent in robotics deployed in space. Figure 6-2 shows what such a system might look like. Although creating systems that work in space presents many significant challenges, the removal of the constraints of gravity would be very beneficial for any MSRR system. Not being constrained by gravity might allow for additional connection mechanisms, in addition to electro-magnetic systems to assist with reconfiguration, as proposed in [44]. One potential implementation of this idea using electro magnets is illustrated by the arrows between the two modules in Figure 6-2, and this could increase reconfiguration reliability significantly.

One of the other areas where the 3D M-Blocks lack development is in the connection mechanism between modules. In order to form practical structures, stronger connections with other modules and the ability to have modules which can assemble passive lattice elements would be very beneficial. Creating a reliable, effective and compact connector is one of the largest unsolved problems in the MSRR field, although there are many potentially interesting avenues to explore in order to develop such a connector. Hopefully the continuation of this work will create a practical MSRR system which, while not as functional as the robots in Hollywood movies, begins to accomplish useful tasks in the real world or in space.

Bibliography

[1] Greg Aloupis, Sébastien Collette, Mirela Damian, Erik D Demaine, Robin Flatland, Stefan Langerman, Joseph O'rourke, Val Pinciu, Suneeta Ramaswami, Vera Sacristán, et al. Efficient constant-velocity reconfiguration of crystalline robots. *Robotica*, 29(1):59–71, 2011.

[2] Byoung Kwon An. Em-cube: Cube-shaped, self-reconfigurable robots sliding on structure surfaces. In *IEEE International Conference on Robotics and Automation (ICRA)*, pages 3149–3155, May 2008.

[3] Nora Ayanian, Paul J White, Adám Hálász, Mark Yim, and Vijay Kumar. Stochastic control for self-assembly of xbots. In *ASME 2008 International Design Engineering Technical Conferences and Computers and Information in Engineering Conference*, pages 1169–1176. American Society of Mechanical Engineers, 2008.

[4] Nadia M Benbernou. *Geometric algorithms for reconfigurable structures*. PhD thesis, Massachusetts Institute of Technology, 2011.

[5] Erik Bjerke and Björn Pehrsson. Development of a nonlinear mechatronic cube. 2016.

[6] Björn Bolund, Hans Bernhoff, and Mats Leijon. Flywheel energy and power storage systems. *Renewable and Sustainable Energy Reviews*, 11(2):235–258, 2007.

[7] Stéphane Bonardi, Massimo Vespignani, Rico Moeckel, and Auke Jan Ijspeert. Collaborative manipulation and transport of passive pieces using the self-reconfigurable modular robots roombots. In *Intelligent Robots and Systems (IROS), 2013 IEEE/RSJ International Conference on*, pages 2406–2412. Ieee, 2013.

[8] Zack Butler, Sean Byrnes, and Daniela Rus. Distributed motion planning for modular robots with unit-compressible modules. In *Intelligent Robots and Systems, 2001. Proceedings. 2001 IEEE/RSJ International Conference on*, volume 2, pages 790–796. IEEE, 2001.

[9] Zack Butler, Keith Kotay, Daniela Rus, and Kohji Tomita. Generic decentralized control for a class of self-reconfigurable robots. In *Robotics and Automation, 2002. Proceedings. ICRA'02. IEEE International Conference on*, volume 1, pages 809–816. IEEE, 2002.

[10] Zack Butler and Daniela Rus. Distributed planning and control for modular robots with unit-compressible modules. *The International Journal of Robotics Research*, 22(9):699–715, 2003.

[11] S Chennareddy, Anita Agrawal, and Anupama Karuppiah. Modular self-reconfigurable robotic systems: A survey on hardware architectures. *Journal of Robotics*, 2017, 2017.

[12] C. Chiang and G. S. Chirikjian. Modular Robot Motion Planning Using Similarity Metrics. *Autonomous Robots*, 10:91–106, 2001.

[13] David Johan Christensen, Ulrik Pagh Schultz, and Kasper Stoy. A distributed and morphology-independent strategy for adaptive locomotion in self-reconfigurable modular robots. *Robotics and Autonomous Systems*, 61(9):1021–1035, 2013.

[14] Sebastian Claici, John Romanishin, Jeffrey I Lipton, Stephane Bonardi, Kyle W Gilpin, and Daniela Rus. Distributed aggregation for modular robots in the pivoting cube model. In *Robotics and Automation (ICRA), 2017 IEEE International Conference on*, pages 1489–1496. IEEE, 2017.

[15] J. Davey, N. Kwok, and M. Yim. Emulating self-reconfigurable robots - design of the smores system. In *Intelligent Robots and Systems*, pages 4464–4469, 2012.

[16] Irene María De Parada Muñoz. Systematic strategies for 3-dimensional modular robots. Master's thesis, Universitat Politècnica de Catalunya, 2015.

[17] Robert Fitch, Zach Butler, and Daniela Rus. Reconfiguration planning for heterogenous self-reconfiguring robots. In *Intelligent Robots and Systems*, pages 2460–2467, 2003.

[18] Robert Fitch and Zack Butler. Scalable locomotion for large self-reconfiguring robots. In *IEEE International Conference on Robotics and Automation*, pages 2248–2253, April 2007.

[19] Robert Fitch and Zack Butler. Million module march: Scalable locomotion for large self-reconfiguring robots. *International Journal of Robotics Research*, 27(3-4):331–343, March/April 2008.

[20] Toshio Fukuda and Seiya Nakagawa. Dynamically reconfigurable robotic system. In *IEEE International Conference on Robotics and Automation*, pages 1581–1586, April 1988.

[21] M. Gajamohan, M. Merz, I. Thommen, and R. D'Andrea. The cubli: A cube that can jump up and balance. In *Intelligent Robots and Systems*, pages 3722–3727, 2012.

[22] Mohanarajah Gajamohan, Michael Muehlebach, Tobias Widmer, and Raffaello D'Andrea. The cubli: A reaction wheel based 3d inverted pendulum. *IMU*, 2(2), 2013.

80

[23] Kyle Gilpin. Distributed algorithms for self dissasembly for modular robots. M.Eng. and S.B. Thesis, June 2006.

[24] Kyle Gilpin and Daniela Rus. Modular robot systems: From self-assembly to self-disassembly. *Robotics and Automation Magazine*, 17(3):38–53, September 2010.

[25] Kyle W. Gilpin. *Shape Formation by Self-Disassembly in Programmable Matter Systems*. PhD thesis, MIT, 2012.

[26] En-guang Guan, Zhuang Fu, Jian Fei, Jia-xin Zhai, Wei-xin Yan, and Yan-zheng Zhao. M-lattice: A self-configurable modular robotic system for composing space solar panels. *Proceedings of the Institution of Mechanical Engineers, Part I: Journal of Systems and Control Engineering*, 229(5):406–418, 2015.

[27] Ferran Hurtado, Enrique Molina, Suneeta Ramaswami, and Vera Sacristan. Distributed universal reconfiguration of 2d lattice-based modular robots. In *29th European Workshop on Computational Geometry*, pages 139–142, March 2013.

[28] Mustafa Emre Karagozler, Jason D Campbell, Gary K Fedder, Seth Copen Goldstein, Michael Philetus Weller, and Byung Woo Yoon. Electrostatic latching for inter-module adhesion, power transfer, and communication in modular robots. In *Intelligent Robots and Systems, 2007. IROS 2007. IEEE/RSJ International Conference on*, pages 2779–2786. IEEE, 2007.

[29] Hiroshi Kawano. Complete reconfiguration algorithm for sliding cube-shaped modular robots with only sliding motion primitive. In *Intelligent Robots and Systems (IROS), 2015 IEEE/RSJ International Conference on*, pages 3276–3283. IEEE, 2015.

[30] B. T. Kirby, B. Aksak, J. D. Campbell, J. F. Hoburg, T. C. Mowry, P. Pillai, and S. C. Goldstein. A Modular Robotic System Using Magnetic Force Effectors. In *Intelligent Robots and Systems*, pages 2787–2793, 2007.

[31] Adam W Koenig, Marco Pavone, Julie C Castillo-Rogez, and Issa AD Nesnas. A dynamical characterization of internally-actuated microgravity mobility systems. In *Robotics and Automation (ICRA), 2014 IEEE International Conference on*, pages 6618–6624. IEEE, 2014.

[32] Michihiko Koseki, Kengo Minami, and Norio Inou. Cellular robots forming a mechanical structure (evaluation of structural formation and hardware design of "chobie ii"). In *Distributed Autonomous Robotic Systems*, pages 131–140, June 2004.

[33] Keith Kotay, Daneila Rus, Marsette Vona, and Craig McGray. The self-reconfiguring robotic molecule. In *IEEE International Conference on Robotics and Automation (ICRA)*, pages 424–431, 1998.

[34] Haruhisa Kurokawa, Satoshi Murata, Eiichi Yoshida, Kohji Tomita, and Shigeru Kokaji. A 3-d self-reconfigurable structure and experiments. In *Intelligent Robots and Systems*, pages 860–865, October 1998.

[35] Haruhisa Kurokawa, Kohji Tomita, Akiya Kamimura, Shigeru Kokaji, Takashi Hasuo, and Satoshi Murata. Distributed self-reconfiguration of m-tran iii modular robotic systems. *International Journal of Robotics Research*, 27(3-4):373–386, March-April 2008.

[36] Michael D.M. Kutzer, Mathew S. Moses, Christopher Y. Brown, David H. Scheidt, Gregory S. Chirikjian, and Mehran Armand. Design of a new independently-mobile reconfigurable modular robot. In *International Conference on Robotics and Automation*, pages 2758–2764, 2010.

[37] Jens Liedke, Rene Matthias, Lutz Winkler, and Heinz Wörn. The collective self-reconfigurable modular organism (cosmo). In *Advanced Intelligent Mechatronics (AIM), 2013 IEEE/ASME International Conference on*, pages 1–6. IEEE, 2013.

[38] Ross MacGregor. Self-propelled device with center of mass drive system, 2017.

[39] B. J. MacLennan. Universally Programmable Intelligent Matter Summary. In *IEEE NANO*, pages 405–408, 2002.

[40] Andrew D Marchese, Harry Asada, and Daniela Rus. Controlling the locomotion of a separated inner robot from an outer robot using electropermanent magnets. In *Robotics and Automation (ICRA), 2012 IEEE International Conference on*, pages 3763–3770. IEEE, 2012.

[41] Jordan Meyer, Nathan Delson, and Raymond A de Callafon. Design, modeling and stabilization of a moment exchange based inverted pendulum. *IFAC Proceedings Volumes*, 42(10):462–467, 2009.

[42] Satoshi Murata, Eiichi Yoshida, Akiya Kamimura, Haruhisa Kurokawa, Kohji Tomita, and Shigeru Kokaji. M-tran: Self-reconfigurable modular robotic system. *Trans. on Mechatronics*, 7(4):431–441, December 2002.

[43] Jonas Neubert and Hod Lipson. Soldercubes: a self-soldering self-reconfiguring modular robot system. *Autonomous Robots*, 40(1):139–158, Jan 2016.

[44] Martin NISSER, Dario IZZO, and Andreas BORGGRAEFE. An electromagnetically actuated, self-reconfigurable space structure. 2017.

[45] Raymond Oung, Frederic Bourgault, Matthew Donovan, and Raffaello D'Andrea. The distributed flight array. In *IEEE International Conference on Robotics and Automation (ICRA)*, May 2010.

[46] Benoît Piranda, Guillaume J Laurent, Julien Bourgeois, Cédric Clévy, Sebastian Möbes, and Nadine Le Fort-Piat. A new concept of planar self-reconfigurable modular robot for conveying microparts. *Mechatronics*, 23(7):906–915, 2013.

[47] Robert G Reid, Loris Roveda, Issa AD Nesnas, and Marco Pavone. Contact dynamics of internally-actuated platforms for the exploration of small solar system bodies. *i-SAIRAS, Montréal, Canada*, pages 1–9, 2014.

[48] John W Romanishin, Kyle Gilpin, Sebastian Claici, and Daniela Rus. 3d m-blocks: Self-reconfiguring robots capable of locomotion via pivoting in three dimensions. In *Robotics and Automation (ICRA), 2015 IEEE International Conference on*, pages 1925–1932. IEEE, 2015.

[49] John W Romanishin, Kyle Gilpin, and Daniela Rus. M-blocks: Momentum-driven, magnetic modular robots. In *Intelligent Robots and Systems (IROS), 2013 IEEE/RSJ International Conference on*, pages 4288–4295. IEEE, 2013.

[50] Daniela Rus and Marsette Vona. A basis for self-reconfiguring robots using crystal modules. In *IEEE/RSJ International Conference on Intelligent Robots and Systems (IROS)*, pages 2194–2202, October 2000.

[51] Daniela Rus and Marsette Vona. Crystalline robots: Self-reconfiguration with compressible unit modules. *International Journal of Robotics Research*, 22(9):699–715, 2003.

[52] David Saldana, Bruno Gabrich, Michael Whitzer, Amanda Prorok, Mario FM Campos, Mark Yim, and Vijay Kumar. A decentralized algorithm for assembling structures with modular robots. In *Intelligent Robots and Systems (IROS), 2017 IEEE/RSJ International Conference on*, pages 2736–2743. IEEE, 2017.

[53] Gregory C Schroll. *Dynamic Model of a Spherical Robot from first Principles*. PhD thesis, Colorado State University. Libraries, 2010.

[54] Eric Schweikardt and Metin Sitti. Stickybricks: An adhesion-based modular self-reconfigurable robotic system, 2007.

[55] Ming-Chiuan Shiu, Hou-Tsan Lee, Feng-Li Lian, and Li-Chen Fu. Design of 2d modular robot based on magnetic force analysis. In *Industrial Technology, 2008. ICIT 2008. IEEE International Conference on*, pages 1–6. IEEE, 2008.

[56] Joseph Shoer and Mason Peck. Reconfigurable spacecraft as kinematic mechanisms based on flux-pinning interactions. *Journal of Spacecraft and Rockets*, 46(2):466–469, 2009.

[57] Aris Skliros and Gregory S Chirikjian. Torsional random-walk statistics on lattices using convolution on crystallographic motion groups. *Polymer*, 48(7):2155–2173, 2007.

[58] Alexander Sproewitz, Aude Billard, Pierre Dillenbourg, and Auke Jan Ijspeert. Roombots-mechanical design of self-reconfiguring modular robots for adaptive furniture. In *Robotics and Automation, 2009. ICRA'09. IEEE International Conference on*, pages 4259–4264. IEEE, 2009.

[59] Alexander Sprowitz, Soha Pouya, Stéphane Bonardi, Jesse Van Den Kieboom, Rico Mockel, Aude Billard, Pierre Dillenbourg, and Auke Jan Ijspeert. Roombots: reconfigurable robots for adaptive furniture. *IEEE Computational Intelligence Magazine*, 5(3):20–32, 2010.

[60] John W. Suh, Samuel B. Homans, and Mark Yim. Telecubes: Mechanical design of a module for self-reconfigurable robotics. In *International Conference on Robotics and Automation*, pages 4095–4101, May 2002.

[61] Cynthia Sung, James Bern, John Romanishin, and Daniela Rus. Reconfiguration planning for pivoting cube modular robots. In *Robotics and Automation (ICRA), 2015 IEEE International Conference on*, pages 1933–1940. IEEE, 2015.

[62] Yosuke Suzuki, Norio Inou, Hitoshi Kimura, and Michihiko Koseki. Reconfigurable group robots adaptively transforming a mechanical structure. In *Intelligent Robots and Systems*, pages 877–882, 2008.

[63] Yosuke Suzuki, Norio Inou, Michihiko Koseki, and Hitoshi Kimura. Reconfigurable group robots adaptively transforming a mechanical structure-extended criteria for load-adaptive transformations. In *Intelligent Robots and Systems, 2008. IROS 2008. IEEE/RSJ International Conference on*, pages 877–882. IEEE, 2008.

[64] Yosuke Suzuki, Yuhei Tsutsui, Masato Yaegashi, and Satoshi Kobayashi. Modular robot using helical magnet for bonding and transformation. In *Robotics and Automation (ICRA), 2017 IEEE International Conference on*, pages 2131–2137. IEEE, 2017.

[65] Blair Thornton, Tamaki Ura, and Yoshiaki Nose. Wind-up auvs: Combined energy storage and attitude control using control moment gyros. In *OCEANS*, pages 1–9, 2007.

[66] M. T. Tolley and H. Lipson. Fluidic manipulation for scalable stochastic 3d assembly of modular robots. In *International Conference on Robotics and Automation*, pages 2473–2478, May 2010.

[67] Tarik Tosun, Jay Davey, Chao Liu, and Mark Yim. Design and characterization of the ep-face. In *IEEE Intl. Conf. on Robotics and Automation (ICRA)*, 2016.

[68] Ronny Votel and Doug Sinclair. Comparison of control moment gyros and reaction wheels for small earth-observing satellites. 2012.

[69] Michael Philetus Weller, Brian T Kirby, H Benjamin Brown, Mark D Gross, and Seth Copen Goldstein. Design of prismatic cube modules for convex corner traversal in 3d. In *Intelligent Robots and Systems, 2009. IROS 2009. IEEE/RSJ International Conference on*, pages 1490–1495. IEEE, 2009.

[70] Paul J White and Mark Yim. Scalable modular self-reconfigurable robots using external actuation. In *Intelligent Robots and Systems, 2007. IROS 2007. IEEE/RSJ International Conference on*, pages 2773–2778. IEEE, 2007.

[71] Paul J. White and Mark Yim. Reliable external actuation for full reachability in robotic modular self-reconfiguration. *International Journal of Robotics Research (IJRR)*, 29(5):598–612, April 2010.

[72] Paul Joseph White. *Miniaturization methods for modular robotics: External actuation and dielectric elastomer actuation.* PhD thesis, University of Pennsylvania, 2011.

[73] Kevin C. Wolfe, Matthew S. Moses, Michael D.M. Kutzer, and Gregory S. Chirikjian. m^3express: A low-cost independently-mobile reconfigurable modular robot. In *International Conference on Robotics and Automation*, pages 2704–2710, May 2012.

[74] M. Yim, W.M. Shen, B. Salemi, D. Rus, M. Moll, H. Lipson, E. Klavins, and G. S. Chirikjian. Modular self-reconfigurable robot systems: Challenges and opportunities for the future. *Robotics and Automation Magazine*, 14(1):43–52, 2007.

[75] Mark Yim, Kimon Roufas, David Duff, Ying Zhang, Craig Eldershaw, and Sam Homans. Modular reconfigurable robots in space applications. *Autonomous Robots*, 14(2-3):225–237, 2003.

[76] Eiichi Yoshida, Shigeru Kokaji, Satoshi Murata, Kohji Tomita, and Haruhisa Kurokawa. Micro self-reconfigurable robot using shape memory alloy. *Journal of Robotics and Mechatronics*, 13(2):212–219, 2001.

[77] Eiichi Yoshida, Satoshi Murata, Kohji Tomita, Haruhisa Kurokawa, and Shigeru Kokaji. Distributed formation control for a modular mechanical system. In *Intelligent Robots and Systems*, pages 1090–1097, 1997.

[78] T Yoshimitsu, T Kubota, and I Nakatani. Operation of minerva rover in hayabusa asteroid mission. In *57th International Astronautical Congress, Valencia/Spain*, 2006.

[79] Mitchell Zakin. The next revolution in materials. In *DARPAâĂŹs 25th Systems and Technology Symposium (DARPATech)*, 2007.

[80] Yanhe Zhu, Jie Zhao, Xindan Cui, Xiaolu Wang, Shufeng Tang, Xueyuan Zhang, and Jingchun Yin. Design and implementation of ubot: A modular self-reconfigurable robot. In *Mechatronics and Automation (ICMA), 2013 IEEE International Conference on*, pages 1217–1222. IEEE, 2013.

Appendix A

Design Documents

This includes schematics for all of the circuit boards in the 3D M-Blocks modules. The first two boards (Arduino controller, and face board) were designed by John Romanishin, while the second two boards (Main board, and Daughter board) were designed by Kyle Gilpin and are included here for completeness.

There is also a partial parts listing for the mechanical components in each 3D M-Block module. The costs in the section are gross estimates and do not account for the significant tooling costs involved with actually ordering these parts. All but two of the non Commercial Off the Shelf (COTS) mechanical components were manufactured at MIT in the CSAIL Machine shop.

SDA-MB P1 P$1

SCL-MB P1 P$1

SDA-FB P1 P$1

SCL-FB P1 P$1

I2C-LED-DRIVER
PCA9553DP/01
8 VDD
7 SDA
6 SCL
5 LED3
LED0 1
LED1 2
LED2 3
VSS 4

R13 10K →RST

R3 100K Q2

R4 10K Q1 S8550

PWR

Goal of this is to turn off Power for the entire board except for the PCA9553

I2C-SWITCH
TS3A24157DGSR
10 V+
9 COM1
8 IN1
7 IN2
6 COM2
NC1 1
NO1 2 →SDA
NC2 3
NO2 4 →SCL
GND 5

6PIN-CONNECTOR
CLP-103-02-F-D
RX
3.3V
1 2
3 4
5 6
TX

Depletion Mode FET BSS126 H6906 - Use Spring pin to 3.3V to Break RX connection to allow ESP-09 to be programmed

RX J$10 FET P$1 P1

Tie to GND to Program

GPIO-0 P1 P$1

Ceramic antenna taken from a similar module. Hope for the best?

CERAMIC-WIFI-ANTENNA
END1 END2
WIFI_ANT
P$1 P$2 C2 10uF

ESP8266-MODULE
3 RX
1 RST →RST
GND
WIFI_ANT 12
VCC 11
CH_PD 10 R6 10K PWR
GND
GPIO14 9 →SCL
TX
GND →GND
GPIO0 4 →GND
GPIO2 5 →SDA
GPIO15 6
GND GND3
GPIO13 7
GPIO12 8
ESP-09
GND2
GND4

R5 100K

D1 Red
R2 10K

AMS-5048B
1 SDA
2 SCL
3 A2
4 A1
5 T1
6 T2
7 T3
PWM 14
GND 13
VDD3V 12
VDD5V 11 →PWR
T4 8
T5 9
T6 10
SDA
SCL

R12-VL6 2.2K
Q3-BSS138-VL6 SDA
R9-VL6 2.2K PWR
2.2K R7-VL6
R10-VL6 2.2K PWR
Q4-BSS138-VL6 SCL

U1-VL6
PWR
IN OUT
EN
GND BP
MIC5219 2.8V
C7-VL6 100nF
C6-VL6 100nF
2.8V

R8-VL6 47K
R11-VL6 47K

TOF-DISTANCE-SENSOR-I2C
VL6180
1 GPIO1
4 GPIO0
5 SCL
6 SDA
AVDD 10
AVDD_VCSEL 8 2.8V
AVSS_VCSEL 9
GND 12

TOF Sensor -Backup to see measure rotation angle of central part to Frame, Could be left unpopulated. Requires 2.8V - Shcematic from https://www.sparkfun.com/products/12785

PWR
C4 100nF C3 10uF
C5 100nF

TEMP-PRESSURE-SENSOR
MPL3115A2LGA8
VDD SCL →SCL
CAP SDA →SDA
GND INT1
VDDIO INT2

This is mostly just for fun, but temp/ altitude could be useful.

C1 10uF

APDS-9301-I2C-LIGHT-SENSOR

AMS5048_SPECIAL

MPU6050_BAREBONES

.022uF
C5_MPU

10uF
C2_MPU

.1uF
C3_MPU

.01uF
C4_MPU

MSL0201RGB
ANODE BLUE RED GREEN
U$17

MSL0201RGB
ANODE BLUE RED GREEN
U$18

MSL0201RGB
ANODE BLUE RED GREEN
U$19

MAIN3.3VREG
VIN VOUT
GND
EN BYP
3.3V_REG_STANDARD

SN74LV1G98_LOGIC_MULTI

PCF8575

R1 100 LEDA
R2 100 LEDB
R3 100 LEDC
R4 100 LEDD

.1uF
C7_PCF

R9 100 G1
R8 100 R1
R10 100 B1
R7 100 R2
R6 100 G2
R5 100 B2

VL53L0X
Time of Flight Sensor
XSHUT AVDDVCSEL
GPIO1 AVDD
SDA AVSSVCSEL
SCL
DNC
VDD: 2.6-3.5V
Op. Temp: -20~70°C
VL53L0X

.1uF_VL5 C6_VL5
VL_SUPPLY

S2P12510_HIGHSIDE
OUT1 IN1
OUT2 IN2
GND
U$36

PAD1_GND_FRAME
PAD2_GND
PAD_SCL_1
PAD_SDA_2
PAD_SCL_2
PAD_FRAME_1

AMS5048_SPECIAL
U$5

U$10 U$13
U$16 U$9 U$11 U$14
U$12 U$15

TITLE: 2017-06-04-faceboard_11
Design by: John Romanishin
REV:
Date: 5/13/2018 5:57 PM
Sheet: 1/1

	Part Name	Technical Details	Source	#	Cost / Module
	Frame Assembly				
1	Main frame panel with integrated edge gears	PEI Resin	Injection Moulding	6	$16
2	Edge diametric neodymium magnet	0.125" x 0.395"	COTS	24	$14
3	Face alignment magnets	0.1" x 0.0625"	COTS	48	$5
4	Flathead screws for corner brackets	2-56 x 0.1875"	COTS	24	$3
5	Metal corner bracket -Standard	0.05" 5052 Aluminum	Custom sheet metal	5	$10
6	Metal corner bracket - coil side	"	Custom sheet metal	2	$10
7	Metal corner bracket - main side	"	Custom sheet metal	1	$1
8	Brass springpin for slipring		COTS	1	$0.1
9	Misc. wires to connect things in the frame		COTS	1	$0.1
10	Custom waterjet press in nut	0.0625" Magnesium	Waterjet	24	$2
11	Neodymium magnet for plane changing attraction	0.125x0.125"	COTS	3	$1
12	Plastic insert to locate three planes	PEEK	CNC Mill	3	$3
13	Bearings to support core diagonal primary axis	0.25" x 0.375" x 0.125"	COTS	2	$2
14	Face printed circuit boards with components	0.02" FR4	PCBa	6	$100
	Flywheel Assembly				
15	Flywheel	12L14 Carbon Steel	CNC Turned	1	$30
16	Motor central shaft	3mm Diameter	COTS	1	$2
17	Magnets for motor rotor	0.1875" x 0.125"	COTS	14	$5
18	Magnetic seperator component	ABS	3D Printed	1	$1
	Core Assembly				
19	Core machined backbone	7075 Aluminum	CNC Milling - 7 Fixturings	1	$10
20	Aluminum machined side - motor side	7075 Aluminum	CNC Milling 3 Fixturings	1	$4
21	Aluminum machined side - coil side	7075 Aluminum	CNC Milling 4 Fixturings	1	$4
22	Motor stator		COTS	1	$10
23	Main power and motor circuit board	0.0625" FR4 6 layers	PCBa	1	$80
24	Coil circuit board	0.0625" FR4 6 layers	PCBa	1	$40
25	Misc. electrical wires		COTS	2	$0.25
26	Custom copper solenoid coil	29 Gauge wire - 300 turns	Custom-wound coil	1	$10
27	Screws to connect stator	2-56 socket cap	COTS	3	$2
28	Ground to SMA electrical springpin		COTS	1	$1
29	Main batteries	125 mAh Lipo	COTS	4	$5
30	SMA bolt to main board nut	2-56" brass nut	COTS	1	$1
31	Motor bearings	3x7x3mm	COTS	2	$0
32	Flanged 3/32x3/16x3/32 Bearings	3/32 x 3/16 x 3/32	COTS	6	$6
33	Brass pinholder and integrated linear bearing	Brass	CNC Milling	1	$5
34	Magnet to attract to frame	0.125" x 0.125"	COTS	1	$0.25
35	Brass threaded insert for SMA wire	2-56	COTS	1	$0.25
36	Bolt to clamp SMA wire to contact	2-56 Socket cap	COTS	1	$0.25
37	Machined brass pad to contact Pin	Brass	CNC Milling	1	$2
38	Machined spacer to insulate brass pad	PEEK	CNC Milling	1	$2
39	Spring pin contact for coil and motor side		COTS	2	$3
40	Plastic machined holder for coil side spring pin	PEEK	CNC Milling	1	$1

41	Wrap around sheet metal cage	Spring steel	Waterjet		
42	Bolts to hold in wrap around cage	2-56	COTS		
43	Machined insulator for coil side primary bearing	PEEK	CNC Milling		
44	Pad for electrical slip ring contact - coil side	Brass	Waterjet		
45	Bearing post for braking mechanism	3/32" 7075 Aluminum	Machined - Lathe	2	$5
46	Shaft spacer for bearing post # 1	0.005" Thick	COTS	2	$1
47	Shaft spacer for bearing post # 2	0.02" Thick	COTS	2	$1
48	Small flathead hold to hold bearing post	0-80	COTS	2	$0.25
49	Small screw to cap the bearing post	0-80	COTS	2	$0.5
	SMA Assembly				
50	SMA plastic tube	PEEK	COTS	1	$0.25
51	Dowel pin to engage SMA to metal Pin	0.0625"	COTS	1	$0.25
52	4" SMA wire	0.01" Diameter	COTS	1	$0.5
53	Metal extending pin	0.125" x 0.375"	Machined - Lathe	1	$2
54	SMA return spring		COTS	1	$1
	Mechanical Brake Assembly				
55	Belt holder left	7075 Aluminum	CNC Mill	1	$1
56	Belt holder right	"	CNC Mill	1	$1
57	Belt holder tiny insert component	"	CNC Mill	2	$1
58	Belt Holder Aluminum Part	"	CNC Mill	2	$4
59	Aluminum Dowel Pin for one way clutch	0.0625" x 0.25"	COTS	2	$0.25
60	Timing belt (primary braking contact element)	MXL - 0.375" wide	COTS++	1	$3
61	Steel flux redirector	0.0625" Steel	Waterjet	1	$0.5
62	Belt Holder to magnet - left side		CNC Mill	1	$3
63	Belt Holder to magnet - right side		CNC Mill	1	$3
64	Brake primary permanant magnets	7/16" x 0.125" N52	COTS	2	$2
65	Steel spheres for jewel bearing	0.0625"	COTS	2	$0.01
66	Plastic flexural spring for jewel bearing	PEEK	CNC Mill	2	$2
67	Magnetic keeper for brake magnetic circuit	0.0625" Steel	Waterjet	1	$0.25
68	Small element to space the brake magnets	0.03" 6061 Aluminum	Waterjet	1	$0.3
69	Bolt to hold spacer to magnetic keeper	0-80	COTS	2	$0.1
				Total Parts	Marginal Cube Cost (No startup fees)
				239	$425.31